

IIM MEMORIAL & AWARD LECTURES ATM-2021

75th Annual Technical Meeting of
Indian Institute of Metals

Date: 14th November 2021

Editorial Team:

Arijit Chakrabarty

Sarbari Ganguly

Rohan Ohri

Ravi Ranjan

Samik Nag

Monojit Dutta

Jointly Organized by:

Indian Institute of Metals Jamshedpur & Kolkata Chapters
and Tata Steel Limited

Professor N. P. Gandhi Memorial Lecture

By Professor Shrikant Joshi



Professor N. P. Gandhi

On the recommendation of Mahatma Gandhi, Professor N P Gandhi was chosen, as the most eminent personality for establishing technological branches of study at Banaras Hindu University by Pandit Madan Mohan Malaviya, founder BHU.

With his pioneering efforts and meticulous organising abilities, Prof N P Gandhi established a composite Unit of Geology, Mining and Metallurgy at BHU in 1919. In 1923 the Department of Mining and Metallurgy came into existence and the first ever bachelor's degree courses in Mining and Metallurgy were started.

Prof Gandhi's vision and untiring efforts resulted in production of high-quality metallurgical engineers well equipped to meet the Challenges of pre and post independent India. Throughout his career he had striven to establish strong industry linkages and maintain high professionalism. After retirement from BHU in 1942 he continued to take active interest in metallurgical profession and founded the Bombay Metallurgical Society and set up the Metallurgical Testing Laboratory at Deolali, Mumbai.

In 1961, the Indian Institute of Metals instituted the Professor N P Gandhi Memorial Lecture to perpetuate the memory of a great teacher and professional. Since 1980, the BHUMET trust now, The Prof N P Gandhi Memorial & Metallurgy Trust at BHU, is a cosponsor of this lecture series.



Professor Shrikant Joshi

Shrikant Joshi is a Professor in the Department of Engineering Science at University West, Sweden with nearly 30 years of experience in areas spanning Surface Engineering, Laser Materials Processing and now also Additive Manufacturing. He is a Chemical Engineer by academic training, having obtained his M.S. and Ph.D. degrees from the Rensselaer Polytechnic Institute and University of Idaho, respectively, in USA. Prior to moving to Sweden, he has had long stints as a Scientist at the Defence Metallurgical Research Laboratory (DMRL) and the International Advanced Research Centre for Powder Metallurgy and New Materials (ARCI). His current areas of research are solution & solution-powder hybrid thermal spraying, high-velocity air-fuel spraying and additive manufacturing. His work has led to many industrial applications, over a dozen patent applications and more than 200 publications in peer-reviewed journals. He is a Fellow of the Indian National Academy of Engineering and of ASM International.

Joys and challenges along a fascinating journey through Surface Engineering

Shrikant Joshi
University West
Sweden

Abstract

Surface engineering refers to tailoring properties of a component to impart performance which cannot be realized either by the bulk material or the surface layer alone. The portfolio of associated technologies that enables this has remarkably expanded over the years and today spans mechanical treatments and surface modifications without any extraneous material addition, compositional changes and chemical treatments in the near-surface region, and deposition of appropriate overlay coatings. Adopting such an approach is increasingly inevitable for a vast majority of industrial applications as well as in every-day life, as the bulk property requirements and surface functionality demands are often distinct and a single material that fulfils both is usually unavailable. Today, use of a suitable surface modification methodology extends to protection of industrial parts that are prone to premature degradation due to phenomena such as wear, oxidation, corrosion, high thermal load etc., enhancing performance of parts routinely exposed to harsh operating environments, and even for decorative/aesthetic purpose. Acknowledging the technological need, excited by the associated opportunities and allured by potential commercial benefits, surface engineering has made enormous advances in recent years. Evolution of new techniques for surface modification and innovations in prevailing methods have ensured immense versatility and an ever-growing application spectrum that already spans nearly every known industry segment.

In this talk, I will attempt to provide a bird's eye view of the interesting canvas offered by surface engineering for pursuing cutting-edge multidisciplinary research and realizing novel applications. Along the way, an insight into the vast portfolio of surfacing options available today to a designer to deliver more durable, versatile, and cost-effective solutions will be provided. I will rely on numerous illustrative examples based on my own experience to highlight the considerable potential of surface engineering as well as some extant challenges.

Dr. Daya Swarup Memorial Lecture

By Professor B. Ravi



Dr. Daya Swarup

Dr Daya Swarup was Principal of the College of Mining and Metallurgy at BHU during 1942 and 1962, a crucial period in the history of the Institution. Following the advent Independence in August 1947, Dr Daya Swarup worked ceaselessly to emphasize the importance of the College and its importance and the role it was destined to play in free India.

For 34 years he worked as a Teacher out of which more than 20 years he was Head of the Metallurgical and Mining Departments. He secured grants from Universities and Government of India to equip laboratories and workshops of the College with latest equipments and instruments. He selected young teachers who had distinguished themselves in College, got them trained abroad, with the result that within a few years BHU had the best equipped Departments of Mining & Metallurgy in the Country.

There is no Mining and Metallurgical activity in India today, where his ex-students have played a key and crucial role in Nation building activities be it in Steel, Non-Ferrous Metals, Mines or Engineering Industry.

In 1989, the Indian Institute of Metals instituted the Dr Daya Swarup Memorial Lecture to perpetuate the memory of a gifted teacher, a warm-hearted person and an able administrator, who loved his profession and his students.



Professor B. Ravi

B. Ravi is Institute Chair Professor of Mechanical Engineering and Head of Desai Sethi School of Entrepreneurship at IIT Bombay. He is Honorary Adjunct Professor at National Institute of Advanced Studies, Bangalore; Fellow of Indian National Academy of Engineering and Abdul Kalam Technology Innovation National Fellow.

Prof. Ravi led or mentored several major projects in metal casting (E-Foundry and SMART Foundry) and medical sector (BETIC, CollabDDS and OrthoCAD). These led to innovative products licensed to startup companies and industry partners. He also shared his knowledge through 260 technical papers, 300 invited talks and 75 training programs. Many institutes are part of BETIC or E-foundry network.

As a member of governing councils of various institutes (Central Manufacturing Technology Institute, Bangalore; Kalam Institute of Health Technology, Visakhapatnam; Sree Chitra Tirunal Institute of Medical S&T, Trivandrum and others), Prof. Ravi guides their vision and strategy. He is also a member of expert committees of many government agencies (AICTE, BIRAC, BIS, DBT, DST, ICMR, MHRD and NITI Aayog), contributing to relevant project reviews and policy recommendations.

Metal Casting 4.0: Closing the Loop between Design and Manufacturing

B. Ravi

Institute Chair Professor, Mechanical Engineering
Indian Institute of Technology Bombay, Mumbai-400076
b.ravi@iitb.ac.in

Abstract

Product quality depends upon symbiotic inter-dependencies among material, design, tooling and process parameters. Such multifarious relationships make it very difficult to avoid defects in metal casting – still the most economical process to produce large parts with intricate features. To get the quality ‘right first time and every time’, we need to transform this art into science by leveraging the latest information technologies. Four relevant R&D works carried out by the author and associates over the last three decades are described in this article: (i) user-friendly simulation software to predict casting defects; (ii) intelligent design and optimization of methoding and tooling; (iii) Cloud-based utilities for ubiquitous access; and (iv) smart foundry for process data capture and analytics. These are laying the path for new technologies to reduce the difference between designed and manufactured products. Such advanced and inter-disciplinary projects are also changing the mind-set about metal casting and attracting the next generation of researchers.

Keywords: Metal Casting, Design for Manufacturability, Process Simulation, Industry 4.0, Smart Manufacturing

1. METAL CASTING

Metal casting represents a major milestone in the long history of humankind. The Rigved mentions casting equipment such as dhatri (cupola) and bhatri (blower). The bronze dancing girl found at Mohen-jodaro, iron pillar in Delhi and pancha-dhatu (five-metal) statues in Chola temples stand testimony to this fine art practiced over millennia [1].

Today, India is among the top three countries worldwide producing a large variety of cast parts for various sectors (Fig. 1). These include transport (automobile, aerospace, railways and shipping), heavy equipment (construction and mining), farming (tractor, irrigation, harvester, dryer), machine tools for various manufacturing processes, plant

machinery (chemical, petroleum, paper, sugar, textile, steel and thermal power), defence (vehicles, artillery, munitions, storage and support), electrical machines (motors, generators, pumps, compressors, transmission and distribution), sanitary (pipes, joints, valves and fittings), household (appliances, kitchen, gardening and fittings), art works (metal sculpture, furniture, lamp-stands and decorations) and medical (diagnostics equipment, surgical instruments and implants).

The above examples establish the versatility of casting process. A variety of metals and alloys (ferrous or non-ferrous) can be melted and led under gravity, pressure or vacuum into appropriate molds (dispensable or permanent) to obtain near-net shape parts. This continues to be the most economical way to obtain intricate shapes in a wide range of size and weight (few grams to hundreds of tonnes). The order quantity can vary from one-off to millions. Large parts with complex external and internal features can be cast with much less skill, energy and material (wastage) compared to machining.



Fig. 1. Metal cast components used in various sectors

Despite the long history and widespread application, cast parts are considered unreliable due to the presence of various defects (Fig. 2). These include external defects (shape, dimensions, features, roughness), internal defects (misrun, cold shut, inclusion, blow hole, gas porosity, shrinkage porosity, hot tear, crack and others) and property defects (physical, mechanical, metallurgical and chemical). These are difficult to avoid due to the multi-physics phenomena (melting, pouring, filling, solidification, cooling and stresses) involving multiple materials (casting, mold, core, etc.) [2]. Metal temperature and mold opacity make it difficult to observe, measure and control the process parameters. As a result, about 5% castings are rejected and

recycled in production foundries; the rejection rate is much higher in jobbing foundries. This is a far cry from parts per million rejections targeted in other manufacturing processes. It is not surprising that metal casting is considered an art, relying on the intuition and skill of experienced foundry engineers.



Fig. 2. Major casting defects related to process phenomena

There is another exacerbating factor. Casting lifecycle has four major stages, which are usually carried out in separate organizations: component design at original equipment manufacturer (OEM); pattern development in tool-room; process planning, casting and fettling in foundry; and component machining in another company. Process planning (also called methoding) includes the design of gating system to lead molten metal into mold cavity and feeding system to compensate solidification shrinkage (Fig. 3). The component design is modified during tooling and methoding to improve its manufacturability. This can increase its weight (typically 5%–15%), which has to be either accepted by the OEM or machined off, implying higher cost. The above factors along with metal and process also affect overall yield – the ratio of component weight to poured weight, which can range from 40% to 80%. While remelting and recycling is an integral part of metal casting, it also implies preventable loss of energy and productivity.

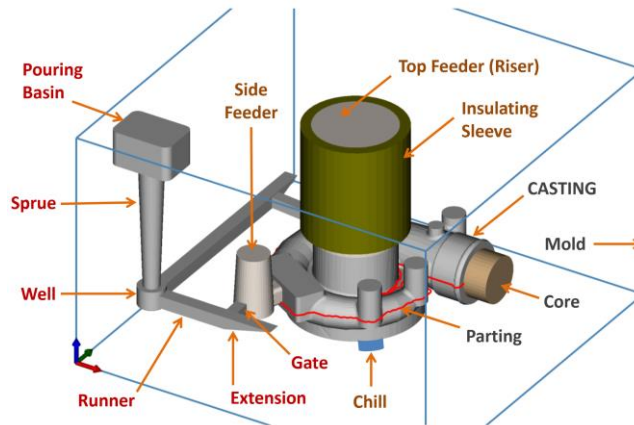


Fig. 3. Casting, mold and methoding (gating and feeding)

Most foundries in India are small and medium enterprises at the bottom of manufacturing value chain as tier-2 or tier-3 suppliers. Their operating margins have been squeezed to single digits due to original equipment manufacturers demanding continuous reduction in price, coupled with rising costs of manufacturing resources – materials, manpower, energy and logistics. This has limited the inflow of capital and human resources required for exploring and implementing new technologies to achieve high quality and optimal yield along with minimal impact on the environment.

Since 1980s, 3D CAD/CAE/CAM technologies have been adapted in the industry, initially by OEMs, followed by others in the value chain. The foundry industry has been slow in this regard. A survey carried out during 2000-2010 involving over 150 Indian foundries showed that only 75% used CAD/CAM and even fewer (25%) used simulation software [3]. Most of them were aware of the benefits of these technologies to minimize internal resources as well as enhance customer value through higher quality assurance and tighter delivery schedules. However, the high cost and difficulty of using the technologies limited their widespread application, particularly in small and medium foundries.

This article describes four relevant R&D works carried out over the last three decades at IIT Bombay and partner organizations. They developed, disseminated and deployed computer-aided technologies for design, simulation, automation and optimization, to successively improve product quality and process efficiency. It started in 1990 with the Gradient Vector Method to quickly predict the location of shrinkage porosity defects. Later, coupled simulation of mold filling and casting solidification enabled predicting many other defects such as blow hole, cold shut and hard zone. The simulation software was integrated with methoding to optimize the design of feeding

and gating systems, and later with tooling design to obtain patterns and core-box models. The basic simulation tool was incorporated in Cloud-based E-Foundry, making it accessible to many people across the world. The last project that is currently underway involves embedding sensors in pattern printing, mold-making, melting & pouring and sand reclamation units to create SMART Foundry. This allows streaming process data to the Cloud, for analysis with respect to product design in terms of quality. The above initiatives and their outcomes are described in the following sections.

2. CASTING PROCESS SIMULATION

Among various casting defects mentioned earlier, solidification shrinkage (in the form of porosity, cavity or sink mark) can account for up to half of the rejections. These occur due to the volume difference between liquid and solid phases of cast metal (up to 7% for aluminium and steel). The shrinkage accumulates at the hot spots, which internally feed adjacent regions that solidify earlier. The defects can be avoided by shifting hot spots into attached feeders, which are later cut-off and recycled (Fig. 4). Small or incorrectly placed feeders can increase the shrinkage defect, whereas overly large feeders reduce the overall yield. For optimizing the feeder design, it is necessary to identify the location and magnitude of hot spots.

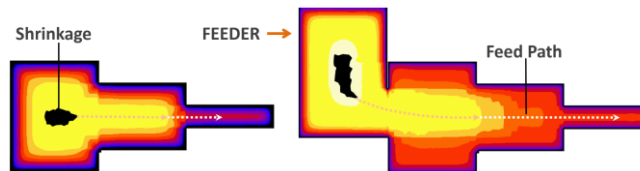


Fig. 4. Shrinkage defect at hotspot, shifted to feeder

The progressive solidification of casting can be simulated using finite difference or finite element methods. The computational domain of casting and mold is divided into many tiny elements; thermo-physical properties (density, thermal conductivity, specific heat and latent heat) are assigned to each element; and boundary conditions, such as the interfacial heat transfer coefficients (at casting-mold, mold-air and other interfaces) are applied. The results are computed by an iterative numerical procedure over a large number of small time-steps. By early 1990s, several simulation programs were available in Europe and USA, adapted by leading foundries [4]. However, input preparation and temperature computation usually took much more time than actual casting solidification. Moreover, the programs were very expensive and required high level of technical skills, limiting their penetration.

By serendipity, a novel method for hot-spot location was discovered in 1988, triggering a chain of technological developments described in this paper. It was based on tracing the directional solidification (the reverse of feed paths), to reach the hot spot [5]. The direction G of maximum solidification at any point P inside the casting is perpendicular to the isothermal contour passing through P and is proportional to the resultant of the thermal flux vectors g_i around P (Fig. 5). The Gradient Vector Method was validated on many shapes from literature, demonstrated for feeder design optimization [6], and successfully applied to industrial castings [7]. The method was continuously improved to handle various boundary conditions such as feeder insulation and casting chill [8].

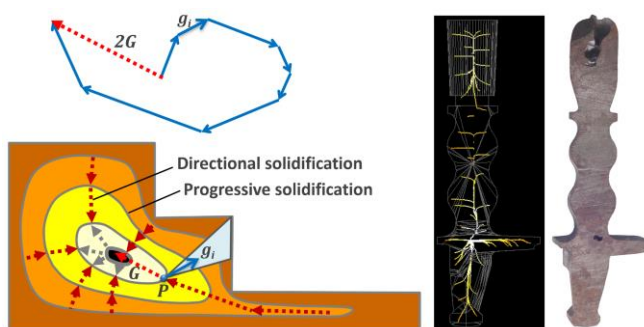


Fig. 5. Gradient Vector Method for feed path simulation

Metal casting is however, a multi-physics process. The liquid metal starts solidifying even before mold filling is complete. Around late 1990s, an all-women team at CSIR-NIIST Thiruvananthapuram started developing the relevant algorithms and created a software called Virtual Casting [9]. The governing equations were based on the conservation of mass, energy and momentum. Additional equations were solved for fluid fraction and boundary conditions at the free surface (its location also being a part of the procedure). The variation of solid fraction between the liquidus and solidus temperatures was handled using Scheil's equation complemented by experimental measurements. The governing equations along with initial and boundary conditions were solved using finite volume method using a structured grid. Explicit time integration scheme for transient simulation was employed, and the time-step for solver computations was automatically selected based on stability criteria. The metal pouring temperature is one of the inputs for mold filling simulation. The computed temperature at the end of filling serves as the initial temperature for solidification simulation.

In 2011, the NIIST team joined hands with IIT Bombay and an industry partner (3D Foundry Tech) to develop an advanced simulation module called FLOW+ with improved features, user interface and computational performance (Fig. 6). The default

inputs including thermo-physical properties and interface heat transfer coefficients are taken from a comprehensive database to minimize user inputs [10]. The mesh generation is also automatic, though the user can control the desired speed and accuracy of results. The software computes mold filling velocity, liquid fraction, solidification temperature and cooling rate at various points inside the casting. These computations take only a few hours for even large and complex castings. The 3D visualization and analysis of results enable accurate prediction of defects related to filling (blow hole, misrun, cold shut), solidification (shrinkage cavity/porosity) and cooling (hard zone). This was successfully validated on several industrial case studies [11].

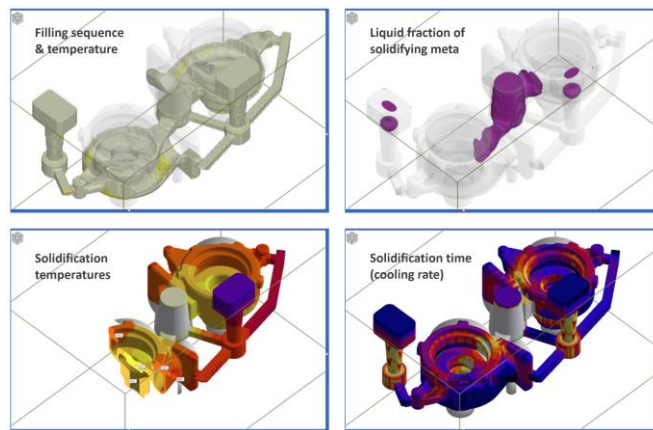


Fig. 6. Coupled simulation of mold filling and solidification

3. METHODING & TOOLING DESIGN

Defect prediction alone is of limited use to foundry engineers. They also need to modify the methoding design in a CAD program, transfer the casting model (along with mold, core, feeding and gating elements) to a simulation program, compute the results, visualize the defects, check if they are still present inside the casting and repeat the steps till the desired quality and optimal yield are achieved. This is cumbersome for those who have limited knowledge, skills and patience for complex software programs. The obvious solution is to integrate casting design and simulation in a single system and incorporate intelligent algorithms to quickly ‘get the job done’ with minimal user inputs.

Methoding of castings is, however, quite complex. It includes many inter-connected decisions regarding mold cavities, gating and feeding (Fig. 3). The number and layout of cavities are optimized to achieve maximum productivity (ratio of cast metal to mold

material per cycle) while minimizing mold damage and casting defects [12]. The gating system comprises pouring basin, sprue, well, runner, extension, gates and filters. Their number, location, shape and dimensions, along with pouring parameters (temperature, pressure, time and rate) are designed to ensure complete, uniform and smooth filling of mold cavity with clean metal. For this purpose, good insights can be derived from experimental studies with water in transparent molds [13]. The elements of feeding system include feeder, neck (connection to casting), sleeve (insulating or exothermic), chill and padding. Feeders can be blind or open to atmosphere; they can be connected to casting top or side. Top feeders have more feeding pressure, but shorter solidification time compared to side feeders. Feeder efficiency can be improved using sleeves or by connecting to multiple castings, as long as there is sufficient capacity (liquid metal in the feeder). Chills can eliminate small local hot spots. The number, location, shape and dimensions of various feeding elements are designed to ensure controlled progressive directional solidification from thin/end regions toward the feeders.

Gating and feeding systems influence each other in many ways. For example, gates connected to side feeders can improve feeding efficiency and reduce fettling effort. On the other hand, thick gates connected to thin sections of casting can lead to local hot spots that may need additional feeders. It is quite common in foundries to experiment with a dozen or more methoding layouts and select the best one after casting experiments (real or virtual). Since the relevant knowledge available in technical literature is limited to simple shapes, the methoding of real-life complex castings remains a practical challenge in foundry industry.

The problem was tackled by systematically collecting and collating the relevant methoding knowledge through deep interactions with senior foundry experts and encapsulating it in rules [14]. One such rule suggests the feeder location (connection point with casting): flat and vertical casting face that is close to hot-spot and mold parting. The feeder dimensions are suggested based on modulus principle: the square of the modulus (ratio of heat content volume to heat transfer area) is proportional to the solidification time of the shape. If the feeder height is close to the mold top, it can be converted into an open feeder. The neck is designed with an intermediate modulus value compared to casting (hot-spot region) and feeder, to ensure directional solidification. All these rules can be incorporated in software algorithms; the user only needs to confirm or fine-tune the suggested values. Then 3D models of the feeder and neck can be generated and attached to the casting. Similarly, gating design would only require the location of gate and sprue by the user; the runner layout, dimensions of all gating elements and generation of their 3D models can be automated [15].

The above approach based on practical methoding knowledge and intelligent geometric reasoning was implemented for the first time in 1998 in a software program called AutoCAST [16]. It empowered even novice engineers (who lack foundry experience) and senior engineers (who may have limited computer skills), to effectively and efficiently use it without elaborate training. Their feedback helped in improving successive versions of the software. Over the next ten years, the software was also employed to train several hundred foundry engineers in casting design and simulation through continuing education programs organized at IIT Bombay.

The tenth version of the software was re-developed with an entirely new user interface, additional features, more automation and expanded alloy database (Fig. 7). It was named AutoCAST-X and launched at the World Foundry Congress at Chennai in 2008. Five years later, an advanced version of the software (AutoCAST-X1) incorporated the FLOW+ module mentioned earlier, which was launched at the Indian Foundry Congress in Ahmedabad. Till date, it has been implemented at about 200 organizations. Most of them are foundries; others include OEMs, R&D institutes and consultants providing simulation services. The end-users reported good matching of simulated and observed results, as well as ease of optimizing the methoding, leading to overall improvement in casting quality, yield and energy utilization.

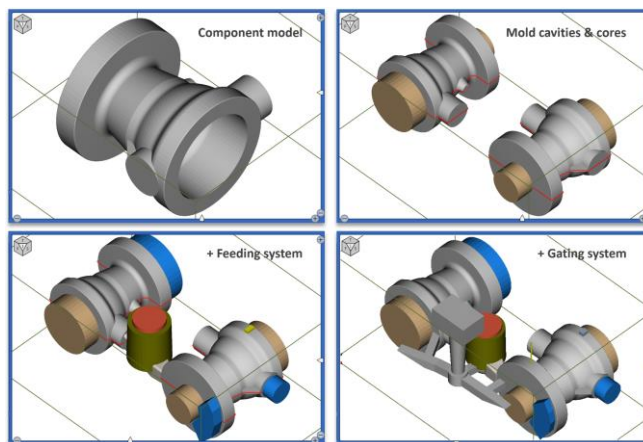


Fig. 7. Semi-automatic design of feeding & gating systems

The next major item on the ‘wish-list’ of foundries was automated tooling design. This had become a bottleneck due to the limited number of tool-rooms and long lead time (often several weeks) for pattern development. Further, poor coordination between tooling and methoding engineers led to many quality issues and increased casting weight, which was unacceptable to OEMs. The activities had to be integrated.

Tooling design has several critical steps. The first is the suppression of drilled holes and other machined features, followed by the twin decisions of casting orientation and mold parting that affect all other steps in tooling and methoding design. Parting line divides the casting surface into non-overlapping regions, each produced by a separate segment of mold – cope, drag or core [17]. It is marked by flash that has to be trimmed later and leaves a visual mark. Cores are designed for through holes and undercuts, which obstruct the withdrawal of the pattern from dispensable mold or casting from permanent mold. Such features can be automatically identified through geometric reasoning [18]. Core supports or prints must be designed for stress as well as transfer of heat and gases. Draft is applied to surfaces perpendicular to the parting (for ease of withdrawal of pattern or casting); more on internal surfaces since they grip the mold. Sharp corners are filleted to facilitate molding and metal flow. Other allowances include contraction, distortion and machining. Their values depend on the casting metal, shape, location and process; they must also follow the standard practices of geometric dimensioning and tolerancing. The allowances can be combined and optimized to reduce the total increase in weight and machining required to obtain the desired component.

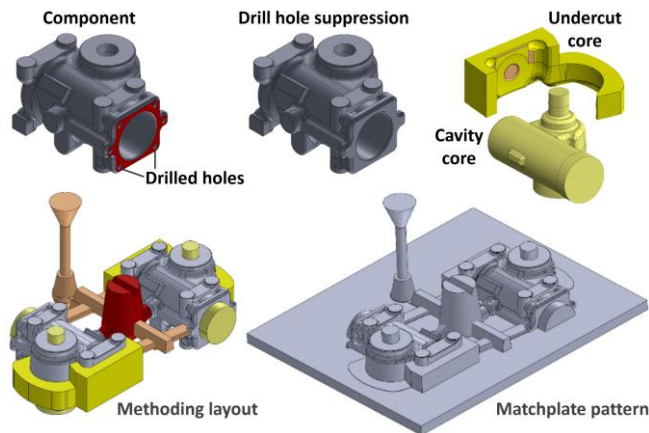


Fig. 8. Tooling (pattern/core) design in CAD environment

The above routines required a regular CAD program. For this purpose, the team selected SolidWorks, since it was widely used and preferred by foundries owing to its user-friendly features for 3D modelling. Using the underlying routines of the software, a new module called AX-Tooling was developed during 2015-2020, to semi-automatically convert a component model into corresponding tooling models (Fig. 8).

Some features of the methoding design and casting simulation mentioned earlier were also included in the module. This was meant for product designers in OEMs to quickly

assess and improve the design for castability [19]. For example, they could minimize hot-spots by redesigning thick junctions, leading to improved quality and yield, as well as reduced weight and machining cost. This was enabled by algorithms for automatic computation of wall thickness [20] and classification of junctions [21]. The availability of tooling, methoding and simulation data made it possible to estimate the tooling cost [22] and casting cost [23]. This enabled early identification and modification of critical features at product design stage itself, to optimize the overall cost.

4. CLOUD-BASED SIMULATION

Indigenous development of technologies brought them within the reach of even small and medium foundries. They were however, constrained by the lack of trained human resources to utilize the software technologies. Most of the engineering and polytechnic institutes had limited resources (teachers and labs) for metal casting theory and experiments. There was a dire need of high-quality learning content in casting design and simulation that could be freely accessed by anyone, anytime, anywhere, using any computing device (desktop, laptop, tablet or smartphone) [24].

This led to the development of a Cloud-based simulation system called E-Foundry during 2012-2015 (Fig. 9). The user can upload a 3D model to the Cloud, and select the cast metal, mold material and mesh size (coarse or fine). The online system computes the solidification results using Gradient Vector Method and sends colour-coded temperature images to the user's device within minutes (Fig. 10). Foundry engineers can identify hot spots (prone to shrinkage porosity), cold spots (prone to cold shuts) and high gradient regions (prone to hot tears); then modify the design, upload the new model and verify by simulation [25]. Product engineers can check and modify the part design (wall thickness, tapers, ribs, fillets) to ensure directional solidification and ease of feeding. Tooling engineers also find it useful to find casting orientations that are easy to feed and fettle.

The system includes several learning resources. 'Classroom' comprises 45 lessons, each with a short video, downloadable slides and online quiz. These are optimized for low Internet bandwidth and smartphone viewing. 'Library' contains process animations, abstracts of over 1000 selected technical papers published worldwide, industrial case studies and defects museum. 'Tutorial' includes 18 exercises in methoding design with immediate feedback. 'Projects' page provides ideas for research in metal casting field. 'Hub' enables discussion threads. All utilities can be freely accessed by the users.

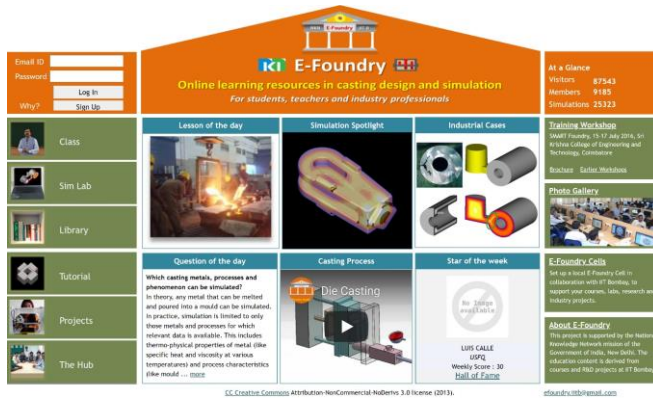


Fig. 9. Cloud-based casting simulation and learning

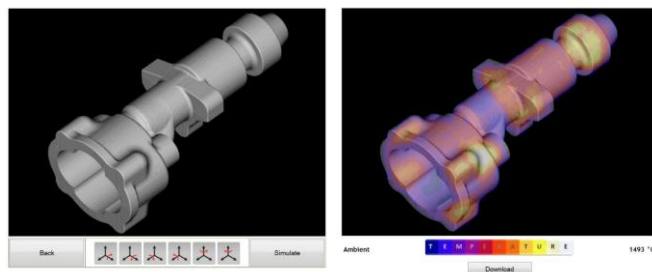


Fig. 10. E-Foundry simulation input and output

Till date, E-Foundry has been utilized by over 9000 members worldwide, who have carried out more than 25,000 simulations. The learning resources were utilized for short training programs at many institutes, benefitting several hundred teachers and students. Some of these institutes later set up dedicated cells for research, training and consulting, leading to closer ties with the local industry.

5. SMART MANUFACTURING

The first three industrial revolutions enabled mass production of complex engineering products (such as automobiles) at low cost, making them affordable to large sections of society. However, they concentrated the activities in clusters, and caused significant damage to the environment. The world started looking for alternate systems of production that are distributed, flexible, smart and sustainable.

The fourth industrial revolution (Industry 4.0) was born out of the convergence of digitization and connectivity. The enabling technologies include automation, simulation, Internet of Things (IoT), Cloud computing, Big data and analytics [26].

The factories of the future will have sensors embedded in all manufacturing equipment that stream data to the Cloud, making it possible to remotely control, visualize, analyse and optimize the process. This would be a great leap forward for countries like India, who already have the necessary IT infrastructure in place.

Industry 4.0 applied to metal casting would enable rapid manufacture of small intricate metal parts with high quality even for single or tiny order quantity, and at much lower cost than conventional casting or metal 3D printing. Driven by this vision, the researchers and industry partners associated with the E-Foundry project conceived SMART Foundry in 2015. They started developing four compact automated units for patternmaking, no-bake molding, melting & pouring and sand reclamation (Fig. 11), with embedded sensors for capturing real-time process data such as temperature and pressure [27].

Pattern-making unit includes a 3D printer developed at College of Engineering, Pune, based on fused deposition modelling process using polymer (ABS or PLA), and a vapour polishing setup to smoothen the surface of fabricated patterns. Sensors pick up the real-time temperatures of the printer nozzle, bed and chamber.

No-bake molding unit was developed by CMERI Durgapur and CMTI Bangalore. It comprises containers for sand and resin, mixing chamber, ramming station, adjustable mold box for match-plate patterns and various actuators. Sensors include load cell for sand discharge quantity, speed sensor for mixer RPM, proximity sensors for ramming station, limit sensor for mold box movement and force sensor for ramming force.

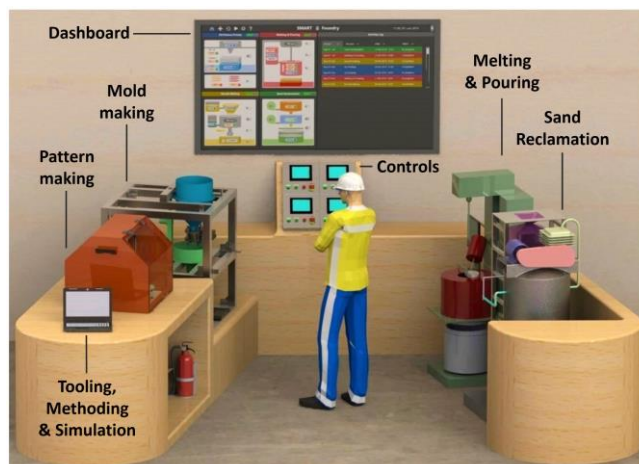


Fig. 11. SMART Foundry units, layout and dashboard

Melting & pouring unit was developed at CHARUSAT, Changa. It combines the two functions to reduce energy loss and improve casting quality. Optional attachments include particle stirring and vacuum pouring. Sensors pick up furnace temperature, pouring temperature, stirrer speed, metal quantity and vacuum chamber pressure.

Sand reclamation unit was developed at DKTE, Ichalkaranji. It comprises lump breaker, vibrating screen, fluidized bed combustor, cooler and sand sieve, and sensors for temperature and other parameters. It can recover 85-90% of no-bake mold sand for reuse in the molding unit.

Microcontrollers placed in all four units collect data from various sensors in real-time and stream it to the Cloud, where it is stored in spreadsheets. A graphical dashboard displays the overall status of the four units and allows the user to view the instantaneous value of any selected parameter or its variation over time. The dashboard is also used for setting the desired values of selected parameters and to switch any unit on or off.

The integrated SMART Foundry (Fig. 12) combines all the technologies developed so far including the software programs for tooling design, methoding design and process simulation; hardware units for pattern-making, no-bake molding, melting & pouring and sand reclamation; as well as process data sensing and monitoring. The first version of the integrated system was put together in 2020 at CMTI Bangalore.

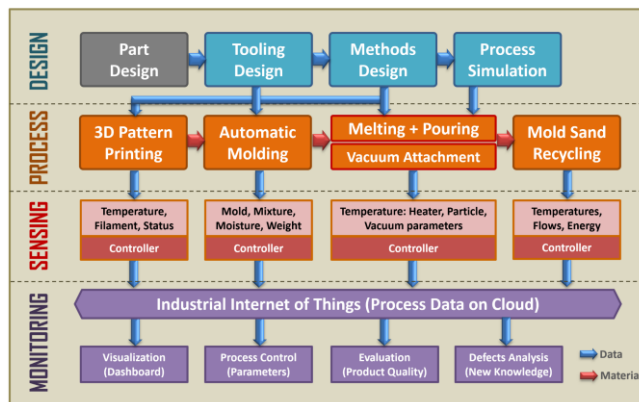


Fig. 12. Integrated software, hardware and IoT for casting

6. CLOSING THE LOOP

Quality is defined as the conformance between designed and manufactured components. The difference between the two cannot be eliminated by improving the manufacturing process alone using conventional techniques such as statistical process

control. It also requires the component design to be compatible with the general capabilities of a selected manufacturing process as well as the specific capabilities of a particular facility or equipment [28].

Product design for manufacturing is an open loop approach; it needs to be replaced by product design for manufacturability, which is a closed loop approach. This requires a comprehensive knowledge base about the effect of a given combination of component geometry, material composition, equipment specifications and process parameters on various aspects of product quality. Measuring and analysing the difference between the designed and manufactured components is the first step in building such a knowledge base. This is enabled by the ‘digital twin’ encompassing the detailed information related to a product and its process.

In metal casting, the component geometry in terms of overall shape, individual features and dimensions is transformed during tooling and methoding design. The manufacturing process (molding, melting, pouring and cooling) creates further divergence in terms of composition, surface quality, internal integrity and mechanical properties. The geometric differences can be visualized by superimposing the 3D scanned model of the cast component over 3D CAD model of the designed component (Fig. 12). The colour mapping of positive and negative deviations provides valuable insights [29].

Such experiments with different combination of component shapes, casting alloys, mold materials and process parameters can help in creating a useful knowledge base to predict the shape and dimensions of new components having a similar combination. The knowledge base incorporated in CAD software will enable fine-tuning the methoding and tooling design (such as distortion and machining allowances) to bring the cast component closer to the designed geometry without shop-floor trials.

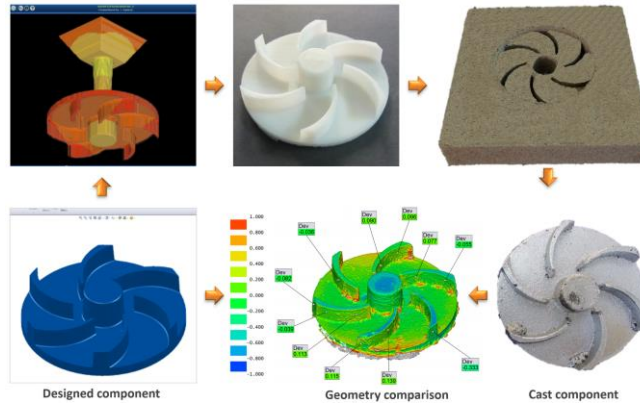


Fig. 12. Geometry comparison of designed and cast parts

The above methodology can be extended to all other aspects of quality. The large amount of process data recorded by sensors embedded in equipment can be mined for useful knowledge. The values of process parameters along with observed defects and mechanical properties can be analysed to identify the parameters (along with their specific range of values) responsible for causing the deviations. For this purpose, AI techniques such as artificial neural networks and Bayesian inference methodology have been found to be useful [30]. The resulting knowledge base will enable optimizing the process parameters to achieve the desired internal quality and mechanical properties for similar castings in the future.

7. CONCLUSION

Even after millennia, metal casting continues to be an essential manufacturing process. This apparently simple process, however, belies complex multi-physics phenomena that defy clear insights. It is very difficult to produce high quality castings without trial and error experiments on the shopfloor. The digital technologies described in this paper are helping unravel the mystery by allowing the visualization and analysis of the component, tooling, methoding, molding filling, solidification and various process parameters on computer before actual casting. The ‘digital twin’ produced by such virtual engineering enables comparing the geometric, material and quality parameters of designed and manufactured components. The resulting knowledge-base is useful for minimizing the future occurrence of defects and deviations.

Closing the loop between design and manufacturing is however, still a work in progress. The paper has hopefully provided a glimpse of the many challenges and opportunities at the intersection of metal casting and information technology fields.

Many new avenues have opened up for inter-disciplinary research, knowledge integration and technology development projects that will benefit the industry as well as the society at large. Long perceived as difficult and dirty, metal casting appears to have crossed the inflection point on the way to becoming smart and sustainable.

ACKNOWLEDGEMENTS

The research work described in this paper spanned three decades and involved more than one hundred researchers, engineers and industry experts from multiple disciplines and organizations. Those who led the projects or made significant contributions deserve special mention. It includes Ramesh Dommeti, who developed the first version of AutoCAST, and Kaustubh Moharir, who developed AutoCAST-X. The tooling design module was created by 3D Foundry Tech team led by BabaPrasad Lanka. The FLOW+ software was developed by Dr. Roschen Sasikumar, Dr. Savithri Sivaraman and Dr. Elizabeth Jacob at CSIR-NIIST, Thiruvananthapuram. Relevant experimental studies were carried out by Dr. MM Akarte, Dr. RG Chougule, Dr. Dinesh Pal, Dr. K. Subburaj, Dr. KH Renukananda and Dr. Himanshu Khandelwal. The E-Foundry project involved Dr. Durgesh Joshi from Indore (who sadly passed away in a road accident), Dr. Mayur Sutaria from Changa, Dr. Amit Sata from Rajkot, and Dr. Vasudev Shinde from Icchalkaranji. The SMART Foundry project brought in additional researchers including Prof. A.M. Kuthe from Nagpur, Prof. Goutam Sutradhar from Kolkata (later Manipur), Dr. Nagahanumaiah from Durgapur (later Bangalore) and Dr. Arati Mulay from Pune. The support of government agencies – National Knowledge Network for E-Foundry project, Department of Science & Technology for the SMART Foundry project, and industry (mainly 3D Foundry Tech) for software development is gratefully acknowledged. The technologies were refined with valuable inputs from many casting experts. The implicit support of the parent institutions of the researchers in sustaining the above projects over many years helped in crossing the ‘valleys of death’ from scientific concepts to practical applications.

REFERENCES

- [1] Ravi B, Metal Casting: Computer-aided Design and Analysis, PHI India, New Delhi, 2005.
- [2] Campbell J, Castings, Butterworth-Heinemann, USA, 2003.

- [3] Ravi B and Joshi D, "10-Year Survey of Computer Applications in Indian Foundry Industry," *Indian Foundry Journal*, 56(1), 2010, 23-30.
- [4] B. Ravi, "CAD/CAM Revolution for Small and Medium Foundries," *Proceedings of the 48th Indian Foundry Congress, Institute of Indian Foundrymen, Coimbatore, 2000.*
- [5] Ravi B and Srinivasan MN, "Hotspots in Castings: Computer-Aided Location and Experimental Validation," *Transactions of the American Foundry Society*, 98, 1990, 353-357.
- [6] Sutaria M, Joshi D, Jagdishwar M and Ravi B, "Feeding System Design and Evaluation using Temperature Gradient (Feed Path) Maps," *Transactions of the American Foundry Society*, 119, 2011.
- [7] Ravi B, "Casting Solidification Feed-path Computation and Industrial Application," *Transactions of the Indian Institute of Metals*, 65(6), 2012, 521-525.
- [8] Sutaria M and Ravi B, "Computation of Casting Solidification Feed-paths using Gradient Vector Method with Various Boundary Conditions," *Int. Journal of Advanced Manufacturing Technology*, 75(1), 2014, 209-223.
- [9] Roschen S, Jacob E, Savithri S, Kumar M and Ravi M, "Computer Simulation of Solidification Processes," *Metal Materials & Processes*, 13(2-4), 2001, 361-368.
- [10] Savithri S, Roschen S, Jacob E, Chourasia V, Sivakumar YVM and Lanka B, "Multi-Physics Simulation and Casting Defect Prediction Using FLOW⁺," *Indian Foundry Journal*, 60(8), 2014, 21-27.
- [11] Ravi B, Savithri S, Roschen S, Marwah AM, "Indigenous Development and Industrial Application of Metal Casting Simulation Software," *Transactions of the Indian Institute of Metals*, 68, 2015, 1227-1233.
- [12] Shinde V, Joshi D, Ravi B and Narasimhan K, "Optimization of Mould Yield in Multi-Cavity Sand Castings," *Journal of Materials Engineering & Performance*, 22(6), 2013, 1558-1564.
- [13] Renukananda KH and Ravi B, "Multi-Gate Systems in Casting Process: Comparative Study of Liquid Metal and Water Flow," *Journal of Materials & Manufacturing Processes*, 31(8), 2016, 1091-1101.
- [14] Chougule RG, Jalan MK and Ravi B, "Casting Knowledge Management for Concurrent Casting Product Process Design," *Transactions of the American Foundry Society*, 112, 2004, 105-114.
- [15] Ravi B, "Intelligent Design of Gating Channels for Casting," *Materials Science & Technology*, 13(9), 1997, 785-790.
- [16] Ravi B, Creese RC and Ramesh D, "Design for Casting – A New Paradigm to Prevent Potential Problems," *Transactions of the American Foundry Society*, 107, 1999.

- [17]Ravi B and Srinivasan MN, “Decision Criteria for Computer-Aided Parting Surface Design,” *Computer-Aided Design*, 22(1), 1990, 11-18.
- [18]Ravi B and Srinivasan MN, “Feature Recognition and Analysis for Molded Components,” *Proceedings of the Int. Conf. on Design Automation*, Coimbatore, India, 1991.
- [19]Ravi B and Srinivasan MN, “Features-Based Castability Evaluation,” *Int. Journal of Production Research*, 33(12), 1995, 3367-3380.
- [20]Subburaj K, Patil S and Ravi B, “Voxel-based Thickness Analysis of Intricate Objects,” *Int. Journal of CAD/CAM*, 6(1), 2006, 101-111.
- [21]Joshi D and Ravi B, “Classification and Simulation based Design of 3D Junctions in Castings”, *Transactions of the American Foundry Society*, 117, 2009, 7-22.
- [22]Nagahanumaiah, Ravi B and Mukherjee NP, “An Integrated Framework for Die/ Mold Cost Estimation Using Design Features and Tooling Parameters,” *Int. Journal of Advanced Manufacturing Technology*, 26(9-10), 2005, 1138-1149.
- [23]Chougule RG and Ravi B, “Casting Cost Estimation in an Integrated Product and Process Design Environment,” *Int. Journal of Computer Integrated Manufacturing*, 19(7), 2006, 676-688.
- [24]Ravi B, “Technical Manpower Training for Foundries: NKN E-Foundry Mission,” *Proceedings of the 60th Indian Foundry Congress*, Institute of Indian Foundrymen, Bangalore, 2012.
- [25]Ravi B, “E-Foundry: Free Online Learning Resources in Casting Design and Simulation,” *Proceedings of the 71st World Foundry Congress*, Bilbao, Spain, 2014.
- [26]Allen D, “Into the 4th Dimension: Industry 4.0 and the Evolution of the Smart Foundry,” *Metal Casting Technologies*, 66(1), 2020, 16-21.
- [27]Ravi B, “SMART Foundry 2020,” *IEEE Potentials*, 35(4), 29-32, 2016.
- [28]Akarte MM and Ravi B, “Casting Product-Process-Producer Compatibility Evaluation and Improvement,” *Int. Journal of Production Research*, 45(21), 2007, 4917-4936.
- [29]Khandelwal H, Gunjal S and Ravi B, “3D Printing Enabled Rapid Manufacture of Metal Parts at Low Cost,” *Indian Foundry Journal*, 62(1), 2016, 47-51.
- [30]Sata A and Ravi B, “Bayesian Inference Based Investment Casting Defects Analysis System for Industrial Application”, *Int. Journal of Advanced Manufacturing Technology*, 90(9-12), 2017, 3301-3315.

IIM - G. D. Birla Gold Medal Lecture

By Professor Rahul Mitra



Shri G.D. Birla

A great leader, Shri G. D. Birla was a reformer, an industrialist, and above all a nationalist. Known for his entrepreneurial spirit and considered a doyen of Indian industry, he laid the foundation of the Birla empire. As a visionary businessman, Shri G.D. Birla has gone down in Indian history as the creator of one of India's largest industrial conglomerates.

Raised in Pilani and Calcutta (now Kolkata), Shri. G.D. Birla forayed into business during World War I. Known for his farsightedness, he was highly vocal about his support towards domestic enterprise and his distaste for foreign capital and foreign goods. He endeavoured to substitute foreign textiles with home-made cloth using the best technology available.

In 1925, along with a group of pioneering industrialists, he set up the Indian Chamber of Commerce, which was closely associated with the Indian Freedom Movement, as the first organised voice of indigenous Indian industry. With Sir Purshottamdas Thakurdas, he co-founded the Federation of Indian Chambers of Commerce and Industry (FICCI). He represented India at the first and second Round Table

conferences in London along with Mahatma Gandhi. In 1945, he was one of the authors of the economic development plan known as the Bombay Plan, a major private sector initiative. The period between 1921 and 1945 was one of the most crucial in Shri G.D. Birla's career, establishing him as the foremost industrialist of pre-independence India.

Shri G.D. Birla wholeheartedly believed in giving. He supported the freedom struggle financially to fulfil the dream of millions of Indians of an independent India. He was also a great believer in the power of education. In 1929, under Birla Education Trust, he set up a primary school focusing on the development of education in Rajasthan. In the 1940s, at the behest of Sardar Vallabhbhai Patel, Shri G.D. Birla contributed to establish the Birla Vishwakarma Mahavidyalaya College in Baroda (now Vadodara). He also contributed for Aligarh Muslim University and helped in setting up the Banaras Hindu University.

Shri. G. D. Birla helped shape the educational trajectory of the country. One of the institutions he founded was the prestigious Birla Institute of Technology and Sciences (BITS), Pilani. A Padma Vibhushan awardee, he also played an instrumental role in setting up several temples, planetariums and hospitals across India.

The G D Birla Gold Medal was established in 1985 in his honour.



Professor Rahul Mitra

Rahul Mitra received B.Tech (Hons.) in Metallurgical Engineering from Indian Institute of Technology, Kharagpur in 1988 and Ph.D. in Materials Science and Engineering from Northwestern University, Evanston, Illinois, USA in 1992. Thereafter, he joined the Defence Metallurgical Research Laboratory at Hyderabad as scientist, and in 2002 he moved to Indian Institute of Technology, Kharagpur, where he is a Professor of Metallurgical and Materials Engineering department, and served as Head from April 2017 to December 2020. He also served as the Head of School of Nano-Science and Technology from October 2016 to December 2020, as the Chairman, Central Research Facility, IIT Kharagpur from December 2009 to November 2017. He has availed of sabbatical leave to carry out research at Northwestern University, Evanston, Illinois and University of Southern California as Visiting Scholar.

At IIT Kharagpur, he has worked on several sponsored projects with net worth of more than INR. 150 Million (USD 2 Million) as Principal Investigator and supervised 23 PhD students. His research is focused primarily on processing as well as structure-property relations of silicide based intermetallic alloys, ultra-high temperature ceramic matrix composites as well as Carbon-fibre-Silicon carbide composites with emphasis on deformation and oxidation behavior for nearly three decades. His research interests also include processing and mechanical behavior of lightweight metal-matrix composites as well as nanocomposite thin films. He has so far 180 publications in peer reviewed journals, 8 book chapters, and two patents (h-index: 35 and i10 index = 104 by Google Scholar). Furthermore, he has authored a book with the title, “Structural Intermetallics and Intermetallic Matrix Composites” published in

2015 by CRC Press, Taylor and Francis Group, and has also edited a book with the title, “Intermetallic Matrix Composites: Properties and Applications”.

He is recipient of the Materials Research Society Medal in 2003, and the Metallurgist of the Year award (Metal Science Category) from the Ministry of Steel, Government of India in 2014. He has been elected as the fellow of the Indian National Academy of Engineering in 2016 and that of the Electron Microscopy Society of India in 2017. He is presently the Chairman of Indian Institute of Metals Kharagpur Chapter, Electron Microscope Society of India East Zone, as well as the Metals and alloys group of the Materials Research Society of India. He is presently a member of the Editorial boards of Sadhana (published jointly by Indian Academy of Sciences and Springer), as well as the Transactions of the Indian Ceramic Society (published jointly by the Indian Ceramic Society and the Taylor and Francis). He has earlier served as a member of the Editorial board of the Transactions of the Indian Institute of Metals and the Bulletin of Materials Science.

Challenges and Breakthroughs in the Development of High temperature Materials

Rahul Mitra

Department of Metallurgical and Materials Engineering
Indian Institute of Technology Kharagpur, Kharagpur – 721302, West Bengal

Abstract

In order to achieve higher energy efficiency and superior performance of engineering components in automotive and aero-engines, thermal and nuclear power industries, various industrial operations, as well as extreme environments experienced in service similar to that by nose-cones and leading edges of hypersonic vehicles, there has been a strong drive for research and development of high temperature materials. High melting point, phase stability, structural integrity and the ability to retain yield and creep strength at high temperature along with a strong resistance to environmental degradation, besides a reasonable amount of fracture toughness or damage tolerance are considered desirable for such materials. The strategies to improve the high temperature capabilities include suitable alloying additions, precipitation and dispersion hardening, addition of ceramic reinforcement, design and use of single crystals, as well as thermomechanical processing. Some of the breakthroughs achieved through the aforementioned approaches in order to meet the challenges of high temperature materials development will be discussed in the present lecture. A significant increase in creep rupture duration along with decrease in creep rate at temperatures up to 300 °C has been noticed in the in-situ Al_{4.5}Cu-5TiB₂ composite subjected to mushy state rolling with prior cold rolling to achieve 30% reduction. Further, precipitation of secondary carbides and their ability to pin the dislocations have been found to contribute to a steady state stage in the tertiary creep regime of the IN617 alloy at 750 and 800 °C, which in turn has extended the rupture life. In research on single crystal Ni-based superalloys, use of the <100> orientation for load application besides suitable alloying additions and heat treatment, has been found to play a key role. Multiphase alloys based on Mo and Nb silicides possess superior high temperature capabilities beyond that of the Ni-based superalloys, with strength retention and oxidation resistance being contributed by the silicide phase, and room temperature toughness by the ductile phase. Alloying of the 76Mo-14Si-10B alloy by Zr has been found to refine the grain size, aiding in rapid formation of a stable and protective borosilicate scaled, thereby improving the oxidation resistance in dry or

moist air. In a similar manner, addition of Ti to the Nb-Si –Mo based alloys along with annealing for 100 h at 1500°C has altered the microstructure with significant increase in room temperature fracture toughness, whereas presence of both Mo and Ti together has improved both high temperature strength and oxidation resistance. The ZrB₂-SiC composite based ultra-high temperature ceramic (UHTC) composites have been found to withstand temperatures >2000°C without significant damage. Pressureless sintering has been developed as a process to fabricate near-net and complicated shapes. Addition of Si₃N₄ to ZrB₂-SiC composites has been found to improve room temperature strength, fracture toughness and oxidation resistance but lower the high temperature creep resistance. On the other hand, addition of ≥10 vol% LaB₆ is found to significantly improve the oxidation resistance in the range of 1300-1500°C by forming a protective scale. The mechanisms of formation of protective scale for oxidation resistance in Mo and Nb silicide-based alloys, as well as the aforementioned UHTCs have been investigated thoroughly, which may help in further development of these materials.

1. Introduction

I begin by sincerely thanking the Indian Institute of Metals for bestowing the honour of G.D. Birla Gold lecture on me. From the days of my undergraduate studies at IIT Kharagpur, and graduate research at Northwestern University, Evanston, Illinois, USA under the guidance of Prof. Morris E. Fine and Prof. Julia Weertman, I have felt an excitement for working on alloys and composites for high temperature applications. Today, I will like to share some of the recent exciting results obtained of my research group at IIT Kharagpur, based on the background of my work carried out earlier as Scientist at DMRL, Hyderabad.

It is well-known that the most desirable properties of materials for use at high temperatures are high melting points, ability to retain strength at the temperature of use, and high creep resistance. Additionally, for materials subject to thermal cycles or gradients, resistance to damage by thermal shock is a necessity. As the environmental degradation sets a major limitation for use at high temperatures in air or corrosive environments, the resistance to oxidation and hot corrosion is an absolute necessity. Furthermore, the ablation resistance is considered essential for use in nose-cones and leading edges of re-entry vehicles. The ascending order of materials based on their high temperature capabilities is as follows: Alloy alloy based metal matrix composites (≤300 °C), Ti alloys and gamma aluminides, 9Cr-1Mo and stainless steels (≤650 °C), Ni- and Co-based superalloys (≤1100 °C), Mo, W and Nb based refractory alloys as well as their silicide based multiphase alloys and C_f/SiC composites (≤1350 °C), MoSi₂ (≤1700 °C), ZrB₂ and HfB₂ based ultra-high temperature ceramic

composites (≤ 1600 °C for long duration, and ≤ 2200 °C for short duration), and C_f/C composites (≤ 2500 °C in vacuum or inert atmosphere only). The research on these high temperature materials is driven by their major applications at different temperature ranges, which include automotive engines, diesel engine glow plugs, boiler tubes and steam turbines in regular and ultra-supercritical power plants, fuel tubes of nuclear reactors, rocket nozzles, hot-end aero engine components, as well as nose-cones and leading edges of hypersonic vehicles.

The strategies to improve the retention of strength at high temperature include alloying for solid solution strengthening, precipitation hardening, dispersion strengthening, evolution of creep resistant phase in a multiphase alloy, design of metal matrix composites with suitable reinforcements, thermo-mechanical processing, and development of single crystal alloys. My research has involved the aforementioned approaches for enhancing the high temperature capabilities without compromising the oxidation resistance along with room temperature toughness. Some interesting results obtained in evaluation of the high temperature properties of selected materials have been discussed, which may contribute to further development.

2. Research on materials development

2.1 Mushy state rolled in-situ Al-4.5Cu-5TiB₂ composite

The process for preparing in-situ Al-TiB₂ composite by mixed salt reaction process was developed at IIT Kharagpur by research group headed by Prof. M. Chakraborty and Prof. B.S. Murty [1]. A major problem encountered in processing cast Al-alloy based metal matrix composites is dendritic structure with segregation of solute at interdendritic locations, and distribution of reinforcement particles to form a grain boundary network, which lead to unsatisfactory mechanical properties. Keeping this problem in mind, a process for rolling of the as cast in-situ Al-4.5Cu-5TiB₂ composite with 20 vol% liquid content to 5% thickness reduction has been developed, which led to significant microstructural refinement with formation of equiaxed grain structure and a more uniform distribution of TiB₂ particles (Fig. 1(a)), which leads to improvement of mechanical properties [2,3]. It has been further noticed that the composite subjected to mushy state rolling with prior cold rolling for 30% reduction (PCMRC) has exhibited the formation of elongated grain structure with a greater number fraction of low angle boundaries, and the best possible distribution of TiB₂ and CuAl₂ particles (Fig. 1(b)), which in turn has significantly improved both tensile strength and ductility at room temperature [4]. As shown in Fig. 1(c), the creep tests on the PCMRC at 275 °C have shown the lowest steady state creep rate with time to rupture of 904 h, which is about three times more than that of mushy state rolled (MRC) and hot rolled composites (HRC) [5]. Additionally, the time to rupture

observed for the PCMRC at 300 °C (260 h) is found to be more by two orders compared to those obtained for both MRC and HRC, as shown in Fig. 1(d). It is found that a large number of low angle boundaries and more evenly distributed CuAl_2 and TiB_2 particles obtained in the PCMRC are considered responsible for higher strength and ductility at room temperature, as well as improved creep resistance at high temperature.

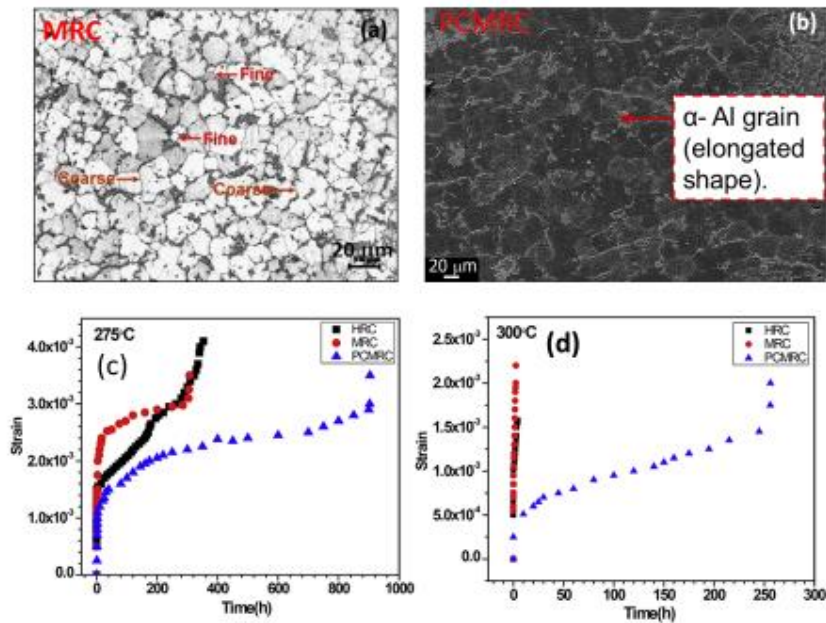


Fig. 1. Optical images showing the effect of mushy state rolling on microstructure: (a) mushy state rolled composite (MRC); (b) Pre-cold rolled mushy state rolled composite (PCMRC); as well as creep properties: (c) plots of creep strain against time for tests carried out at 275 °C; and (d) plots of creep strain against time for tests carried out at 300 °C [4,5].

2.2 Ni-based superalloy

2.2.1. Non-classical creep behaviour of IN 617 alloy

Creep tests on the IN617 alloy at temperatures in the range of 650 – 800 °C have shown (i) creep curves indicating non-classical creep behaviour with a distinct steady state stage with a locally minimum and constant creep rate in the tertiary part of the creep curve at 750 and 800 °C (Fig. 2(a-b)); as well as (ii) values of apparent stress exponent (n) much higher greater than 4-5 (Fig. 2(c)), which is expected for dislocation climb controlled creep [6]. By plotting the (creep rate)^{1/n} against the

applied stress (σ), followed by extrapolation of the best-fit line to $\sigma = 0$, the values of threshold stress (σ_0) at different temperatures have been obtained (Fig. 2(d)). Based on the results obtained from transmission electron microscopy, the threshold stress is ascribed to the interaction of dislocations with γ' precipitates and $M_{23}C_6$ particles dispersed in the microstructure. The plot of creep rate against $\sigma - \sigma_0$ shows n in the range of 4-5 (Fig. 2(e)). Additionally, the threshold stress has been found to decrease with increasing temperature. The appearance of the steady-state stage in the tertiary portion of the creep curves is ascribed to the formation of secondary $M_{23}C_6$ precipitates during creep test at 750 and 800 °C. As shown in Fig. 2(f), interaction of dislocations with secondary $M_{23}C_6$ precipitates is responsible for strengthening during the steady stage of tertiary creep.

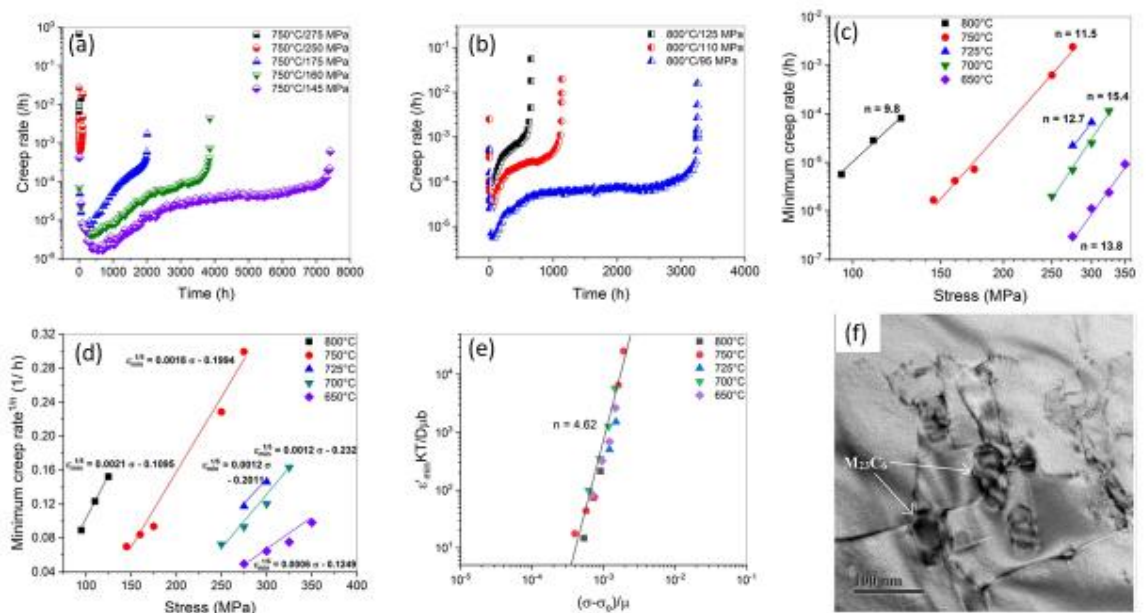


Fig. 2. Results of creep tests on the IN617 alloy: the plots of creep rate against time for creep tests carried out at (a) 750 °C, and (b) 800 °C; (c) log-log plots of minimum creep rate against stress (σ) with best-fit lines to find apparent stress exponent (n); (d) plots of $(\text{min. creep rate})^{1/n}$ against stress to find threshold stress (σ_0); (e) plot of temperature compensated creep rate against $(\sigma - \sigma_0)$ to find true value of n , and (f) TEM image showing interaction of dislocations with $M_{23}C_6$ particles during creep test at 800°C under an applied stress of 125 MPa.

2.2.2. Creep behaviour of a single crystal Ni-based superalloy

The single crystal Ni-based superalloy (DMS4M) containing Cr, Co, W, Re, Ta, Hf, Nb and Al, as developed at DMRL Hyderabad, shows a microstructure containing coherent γ' precipitates with cube-on-cube orientation relations being dispersed in the γ matrix (Fig. 3(a)) [7]. The creep curves have exhibited the predominance of tertiary stage, and the creep resistance observed for the crystals with stress axis along $\langle 100 \rangle$ have been found to be much superior compared to those having $\langle 110 \rangle$ orientations, as shown in Fig. 3(b). Based on the plots of stress against the Larson-Miller parameter, the DMS4M alloy has creep resistance comparable with or superior to those of other second or third generation single crystal alloys including CMSX-4, Rene N5, CMSX-10, and Rene N6, as shown in Fig. 3(c). The raft formation has been found as the primary damage mechanism during creep. Additionally, the coarsening with growth of rafts has been found to be along normal to stress axis for creep with stress axis along $\langle 100 \rangle$ (Fig. 3(d)), and at 45° for stress axis along $\langle 110 \rangle$ (Fig. 3(e)), indicating that the preferred direction of coarsening of the γ' precipitates is $\langle 100 \rangle$. The raft thickness has been found to decrease with increasing applied stress, as shown in Fig. 3(f).

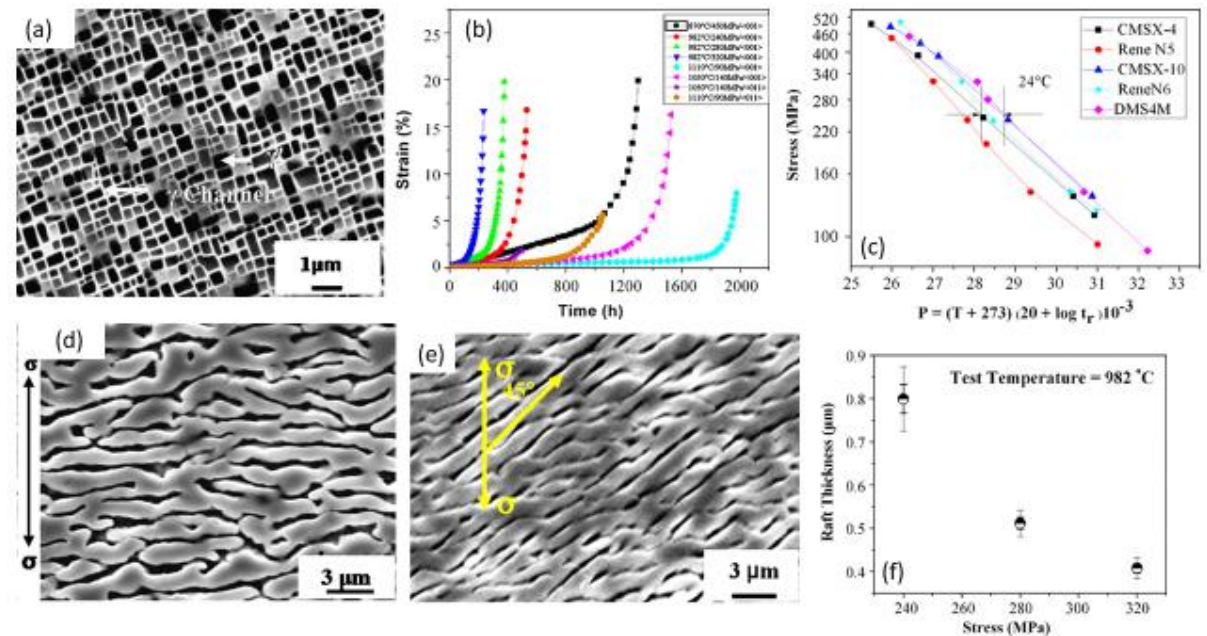


Fig. 3. Microstructure and creep behaviour of DMS4M single crystal Ni-based superalloy [7]: (a) SEM image depicting the microstructure showing cuboidal γ' precipitates; (b) plots of creep strain against time showing the predominance of

tertiary creep; (c) plots of stress against the Larson-Miller parameter with the results obtained for other alloys of similar nature; SEM images indicating growth of rafts in a direction (d) perpendicular to stress axis for loading along $\langle 100 \rangle$ direction, and (e) at 45° to the stress axis (i.e. along $\langle 110 \rangle$) for loading along $\langle 110 \rangle$; as well as (f) plot showing decrease of raft thickness with increase in stress.

2.3 Development of Mo and Nb silicide-based alloys for use beyond Ni-based superalloys

The class of refractory silicide based intermetallic alloys most widely studied are based on Mo and Nb-silicides, which have occupied a major focus of my research for the last three decades.

2.3.1 Structure-property relations of Mo-Si-B alloys

2.3.1.1 Microstructure and mechanical properties

The Mo-Si binary equilibrium phase diagram shows the existence of Mo_3Si with cubic (A15 (strukturbericht), cP8 (Pearson symbol) structure) structure, as well as Mo_5Si_3 (D8_m, tI32) and MoSi_2 (C11_b, tI6) with tetragonal structure (Fig. 4) [8,9]. The melting points of Mo_3Si , Mo_5Si_3 and MoSi_2 are 2025 °C, 2180 °C, and 2020 °C, respectively. Due to the complex crystal structure with low symmetry, the number of slip systems is less than 5, and the Peierls stress is high in the aforementioned Mo-silicides, which is responsible for their intrinsic brittleness, high brittle to ductile transition temperature (≥ 1100 °C), as well as low fracture toughness (2-4 $\text{MPa}\sqrt{\text{m}}$). Still, a significant attention has been paid to develop MoSi_2 as a high temperature structural material, because of its outstanding oxidation resistance till 1700 °C due to the formation of a continuous, stable and protective scale of SiO_2 . By addition of ceramic reinforcement like SiC or Al_2O_3 to MoSi_2 , a marginal increase in fracture toughness is observed, as the crack paths become more tortuous due to crack deflection, crack bridging (Fig. 5(a)). Additionally, the yield strength decreases sharply with increasing temperature, as shown in Fig. 5(b) [10,11].

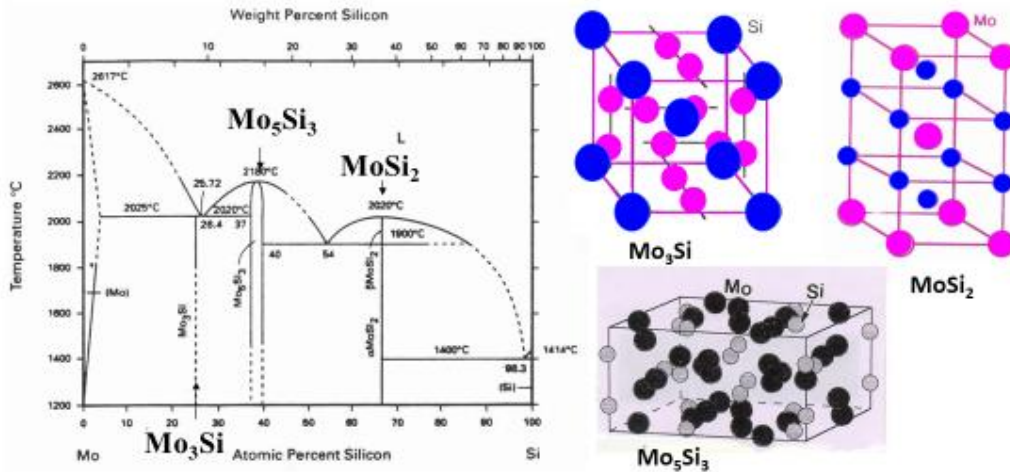


Fig. 4. The Mo-Si binary equilibrium phase diagram showing the composition and melting points of the intermetallics, as well as schematic illustrations of the crystal structures of Mo_3Si (A15), Mo_5Si_3 (D8₈) and MoSi_2 (C11_b) [8,9].

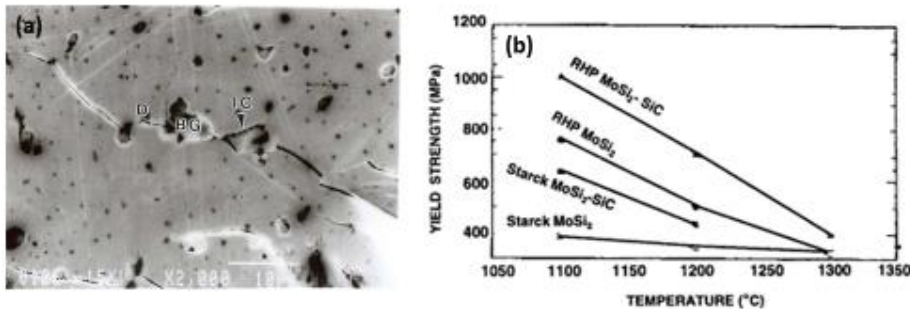


Fig. 5 (a) Deflection and bridging of crack originating from indentation corner in MoSi_2 -5.5Al alloy containing Al_2O_3 particles [10]; (b) plots depicting the variation of yield strength with temperature [11].

Keeping the aforementioned limitations of the addition of ceramic reinforcement in mind, an approach involving the development of Mo-Si-B alloys leading to the formation of Mo_{ss} (Mo-rich solid solution), Mo_3Si and Mo_5SiB_2 as the constituent phases as predicted by the ternary equilibrium isotherm for 1600°C in Fig. 6(a) [12], has been pursued since the late 1990s [8,13]. Such an approach was triggered by the finding that the Mo_5Si_3 with 2 wt% B and Mo_5SiB_2 possess superior oxidation resistance due to the formation of a protective scale of borosilicate glass [14]. Additionally, the creep resistance of Mo_5SiB_2 single crystal has been found to be greater than that of MoSi_2 by three times [15]. In the Mo-Si-B system, the Mo_{ss} being a ductile phase contributes to the enhancement of fracture toughness, whereas Mo_3Si and Mo_5SiB_2 contribute to the retention of high temperature strength along

2.3.1.2 Oxidation behaviour

On isothermal exposure of the 76Mo-14Si-10Nb alloy at temperatures in the range of 800-1300°C, an initial mass loss followed by a regime of reduced or negligible mass change has been observed, whereas almost continuous mass loss has been noticed at 700°C [18]. The oxidation resistance is ensured by the formation of an oxide scale having the borosilicate glass as its outermost layer, which completely arrests the mass loss, as shown in Fig. 8(a). Studies involving short duration isothermal oxidation experiments at 1150°C from 20 s onwards have shown that the surface of this alloy to be covered completely with the borosilicate glass (BSG) within 480 s, provide complete protection against further degradation, as shown in Fig. 8(b) [19]. As the MoO₃ formed by the oxidation of the Mo_{ss} phase vaporizes, cavities are left behind, which are filled by the viscoplastic flow of BSG formed by oxidation of the surrounding Mo₃Si Mo₅SiB₂ phases. The viscoplastic flow of the BSG during isothermal exposure at 1150°C could be confirmed from the formation of ripples in the oxide scale, as shown in Fig. 8(c).

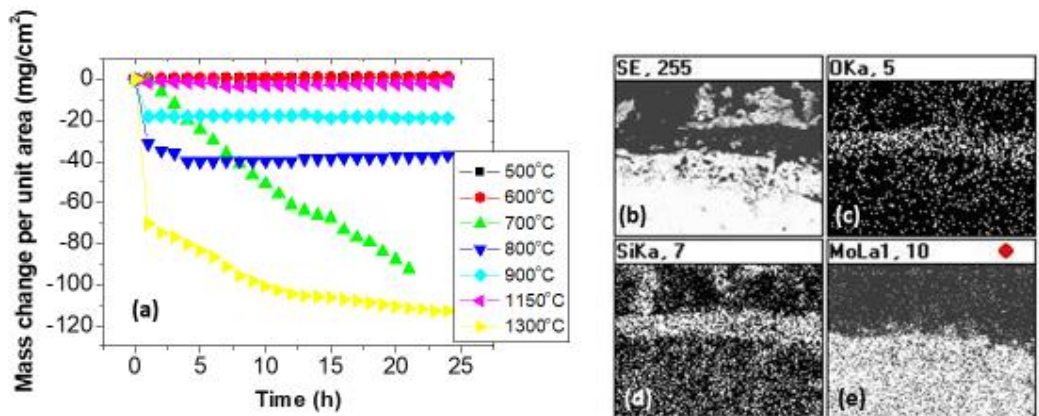


Fig. 7(a) Plots of mass change against time obtained from isothermal oxidation tests carried out in the range of 500-1300 °C on the 76Mo-14Si-10B alloy [18]; (b) SEM (BSE) image of the oxide scale along with EDS X-ray maps of (c) O, (d) Si and (e) Mo.

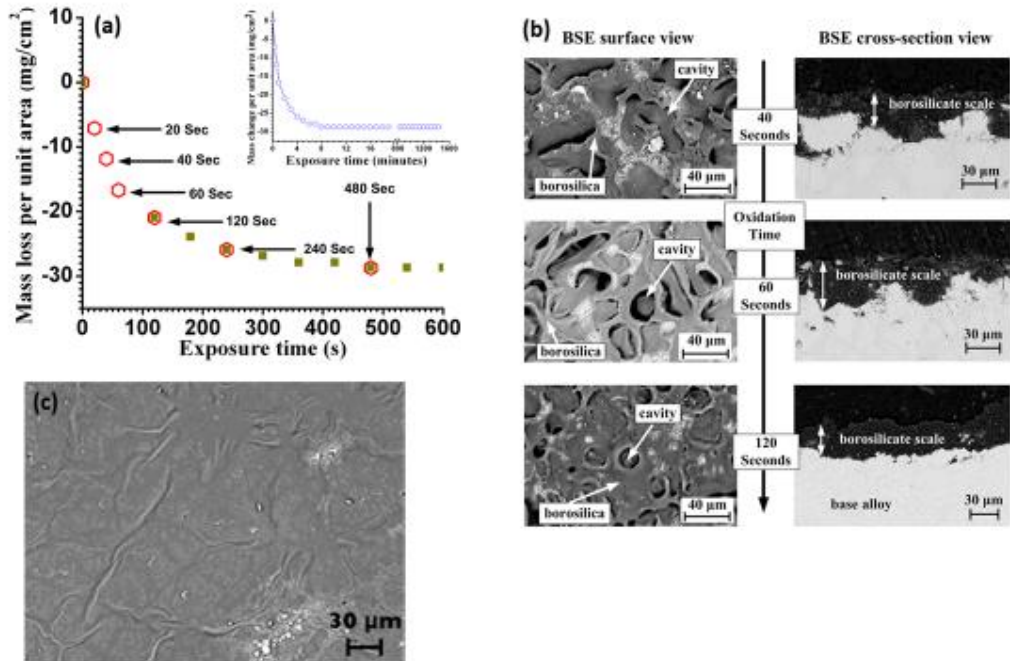


Fig 8. Initial stages of exposure of the 76Mo-14Si-10B alloy at 1150°C: (a) Plot of mass loss per unit area against time of exposure with inset showing the data recorded for 24 h; as well as SEM images showing (b) the top surfaces and oxide scale cross-section showing the cavities formed by oxidation of Mo_{ss} phase with formation and escape of MoO_3 (g), along with filling up of the cavities by the flow of surrounding borosilicate glass formed by oxidation of Mo_3Si and Mo_5SiB_2 ; as well as (c) ripples formed by viscoplastic flow of the borosilicate glass during isothermal exposure [19].

Experiments with addition of 2 at% Zr at the expense of Mo to the aforementioned alloy as well as processing by spark plasma sintering instead of arc-melting have shown a significant refinement of grain size (Fig. 9) along with noticeable decrease in the net mass loss (Fig. 10) [20]. Such an observation has been considered partly due to the refinement of grain size, which by increasing the grain boundary and interfacial area fraction provides rapid diffusion paths for Si and B to the surface, leading to the formation of a protective scale. Additionally, the Zr acts as a glass network modifier, and restricts devitrification. Further, the rapid consumption of MoO_3 to form the $\text{Zr}(\text{MoO}_4)_2$ arrests the mass loss by its vaporization, whereas the formation of ZrSiO_4 lowers the amount of ZrO_2 in the oxide scale, and thereby limit the damage caused by the stresses generated owing to its phase transition. During exposure in moist air in the temperature range of 1000-1300 °C, greater mass loss compared to that in dry air along with the formation of cavities is found in the oxide scales due to vaporization of hydrated MoO_3 and SiO_2 . However, formation of

Zr(MoO₄)₂ and ZrSiO₄ (Fig. 10(f)) along with strengthening of the glass network in the BSG and inhibition of devitrification in the oxide scales of the Zr containing alloys, are considered to have lowered mass loss by vaporization of hydrated MoO₃ and SiO₂, as well as the formation of cavities [21].

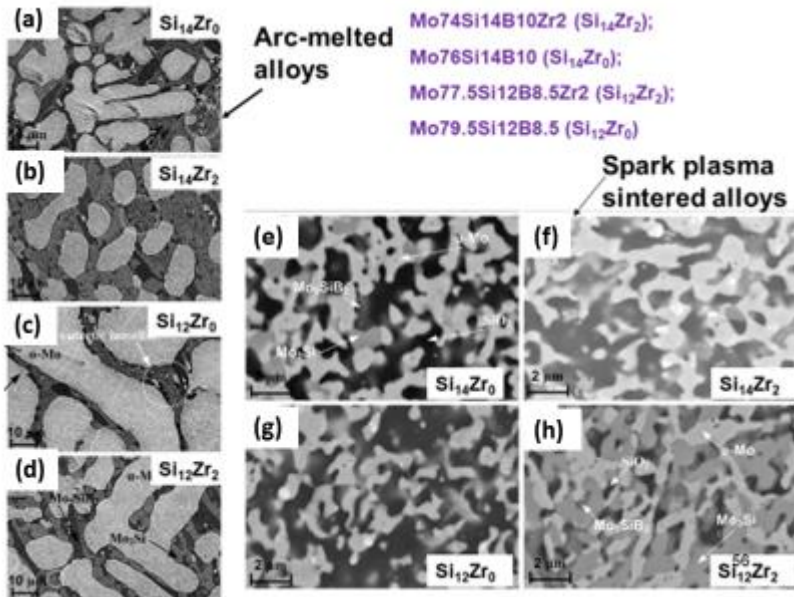


Fig. 9. SEM images depicting the microstructures of (a-d) arc-melted and (e-h) spark plasma sintered Mo-Si-B and Mo-Si-B-Zr alloys [20].

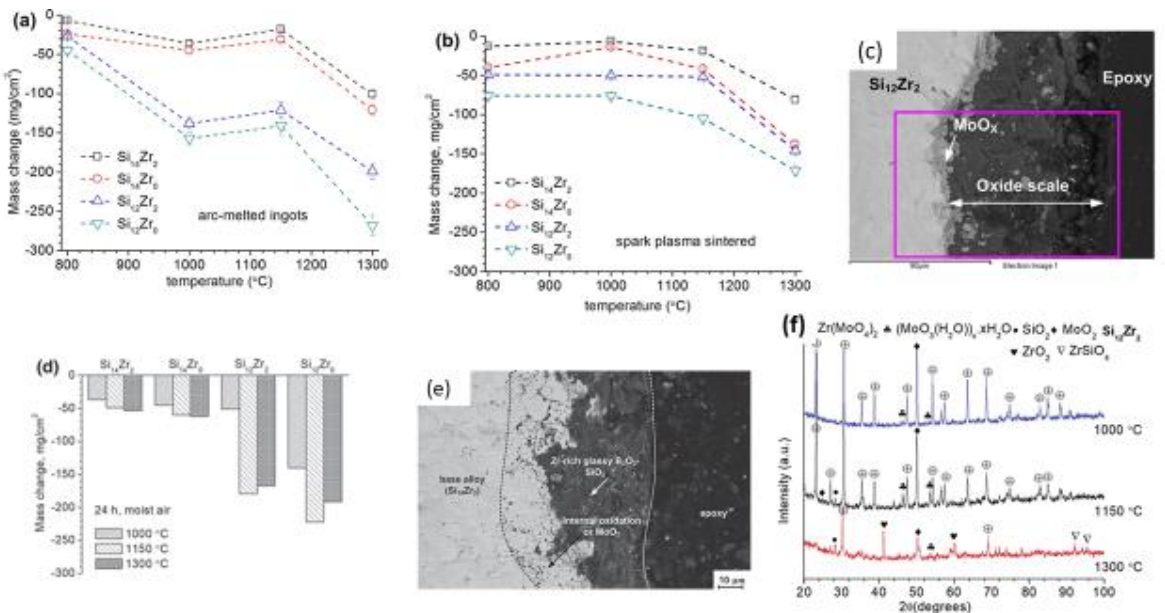


Fig. 10. Plots of mass change with temperature on isothermal exposure for 24 h in dry air at temperatures between 800 °C and 1300 °C for (a) arc-melted and (b) spark plasma sintered Mo-Si-B and Mo-Si-B-Zr alloys; (c) cross-section of the oxide scale

formed at 1000 °C; (d) bar-charts showing mass change on exposure in moist air at temperatures between 1000 °C and 1300 °C; (e) SEM image depicting the cross-section of the oxide scale formed in moist air at 1300 °C; and (f) XRD patterns from oxide scales formed in moist air [21].

2.3.2 Structure-Property relations of Nb-silicide based alloys

2.3.2.1 Nb-Si-Mo alloys

The Nb-Si binary equilibrium phase diagram contains the intermetallics, Nb₃Si, Nb₅Si₃ and NbSi₂, along with a eutectic at 17.5 at% Si (Fig. 11(a)) [22]. A considerable attention has been paid to the Nb-rich binary, ternary and multicomponent alloys with their microstructures being constituted by a mixture of Nb_{ss} and 5-3 silicide (based on Nb₅Si₃). In the present study, the Mo has been preferred as the ternary alloying element, because it is known to (i) form an isomorphous solid solution with Nb; (ii) make the diffusion kinetics sluggish; (iii) inhibit the formation of Nb₃Si as an additional brittle phase [23]; and (iv) stabilize the 5-3 silicide phase [24]. The microstructures contain a eutectic mixture of Nb_{ss} and 5-3 silicide phase, along with Nb_{ss} or 5-3 silicide as the primary phase in the alloys having hypoeutectic or hypereutectic compositions, respectively [25]. Besides the well-expected lamellar morphology, a part of the eutectic colonies in the Nb-Si-Mo alloys also appear non-lamellar and coarse due to the decoupled growth of Nb_{ss} and 5-3 silicide during solidification, being facilitated by large undercooling and complex crystal structure of the 5-3 silicide phase. The non-lamellar eutectic is found to be more effective in arrest and bridging of cracks, which contribute to toughening (Fig. 11(b)) [26]. The compression tests carried out at the strain rate of 10⁻⁴ s⁻¹ on hypoeutectic and hypereutectic alloys at room temperature and 1200°C (Fig. 11(c)) have led to the following inferences [27]: (i) the hypereutectic alloys have higher strength; (ii) the Mo content has little influence on the compressive strength of the hypereutectic alloys; and (iii) the compressive strength of hypoeutectic alloys scales with the Mo content indicating the role played by its solid solution strengthening of the Nb_{ss} phase. The oxidation kinetics at 1000°C has been found to follow a parabolic rate law (Fig. 11(d)), with the mass gain being lower for the alloys with hypereutectic compositions, and further reduced with increase in the Mo content [28]. In the oxide scale of the alloy with higher Mo content (15 at%), formation of a continuous layer of SiO₂ at the alloy-oxide interface is considered to have contributed to the formation of a protective scale (Fig. 11(e)).

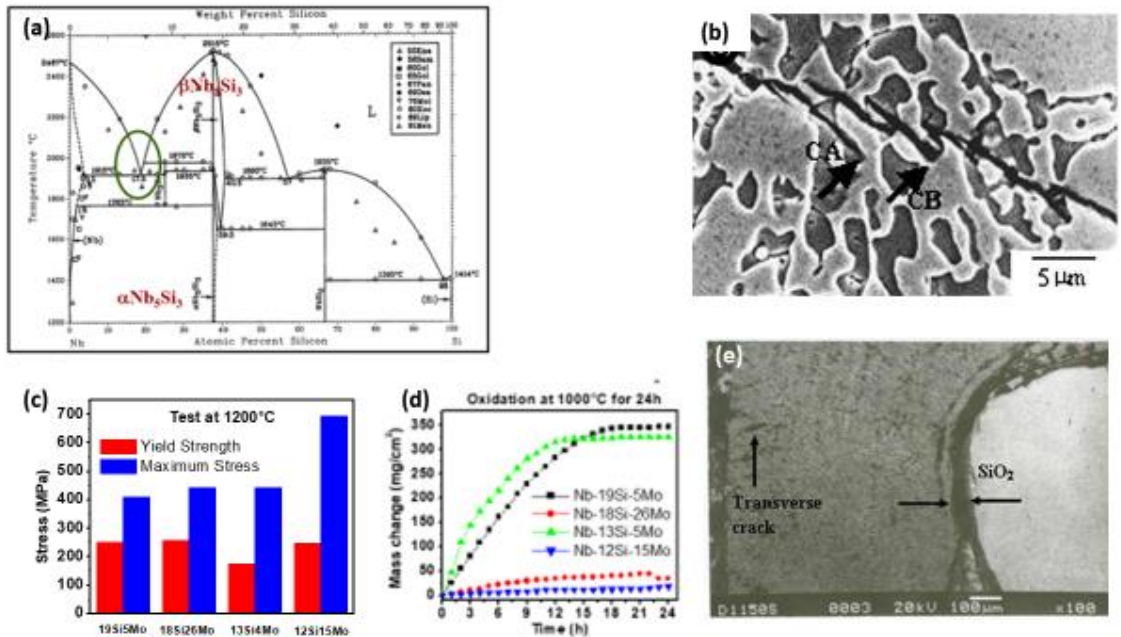


Fig. 11(a) Binary equilibrium phase diagram of the Nb-Si system showing the positions of intermetallics [22]; (b) path of indentation crack through the non-lamellar eutectic in the Nb-13Si-4Mo alloy [26]; (c) Bar charts showing yield strength and maximum stress obtained by compression tests at 1200 °C on hypoeutectic and hypereutectic Nb-Si-Mo alloys [27]; (d) Plots depicting the variation of mass change with duration of isothermal exposure at 1000 °C [28]; and (e) SEM image depicting the formation of a continuous and protective SiO₂ layer at the alloy-oxide interface in the cross-section of the oxide scale formed at 1000 °C on the Nb-18Si-26Mo alloy [28].

2.3.2.2 Effect of 20 at% Ti addition to Nb-Si-Mo alloys

On addition of 20 at% Ti to Nb-12Si-5Mo and Nb-19Si-5Mo alloys, the following changes have been observed in the microstructure (Fig. 12): (i) formation of $\beta\text{-Ti}_{ss}$ with Nb in solid solution, and (ii) increase in the amount of eutectic with non-lamellar morphology in comparison to lamellar eutectic [29, 30]. Additionally, annealing at 1500 °C for 100 h has led to the complete transformation of the eutectic from lamellar to non-lamellar morphology. The fracture toughness values obtained for the hypoeutectic alloys with the ductile Nb_{ss} as the primary phase have been found to be greater than those of the corresponding hypereutectic alloys (Fig. 13(a)) [31]. A significant increase in fracture toughness by 75% and 63% has been observed, respectively on addition of 20 at% Ti and annealing, with the observed maximum

value of fracture toughness being $\sim 14 \text{ MPa}\sqrt{\text{m}}$. The observed increase in fracture toughness is considered to be due to the deviation of crack path from mode I propagation at the $\text{Nb}_{\text{ss}}/5\text{-}3$ silicide interface (Fig. 13(b-d)).

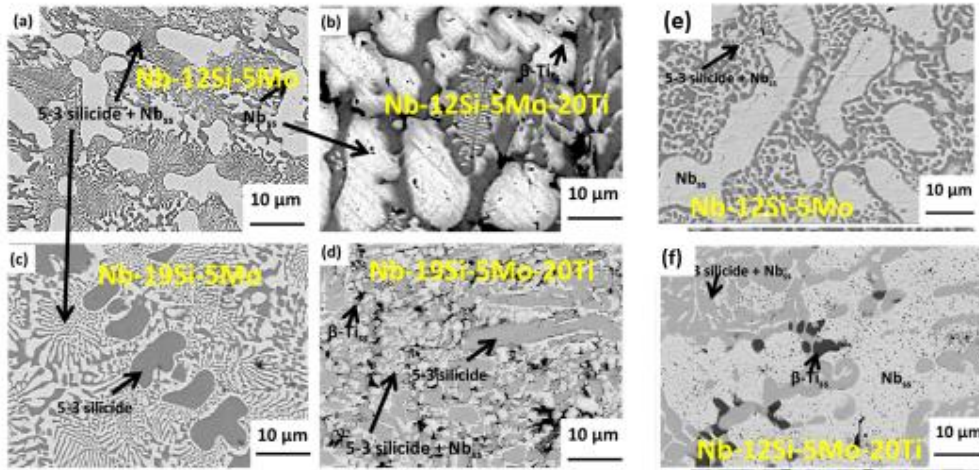


Fig. 12. SEM (BSE) images depicting the microstructures of the arc-melted alloys with compositions: (a) Nb-12Si-5Mo, (b) Nb-12Si-5Mo-20Ti, (c) Nb-19Si-5Mo, (d) Mn-19Si-5Mo-20Ti, as well as post-anneal (1500°C for 100 h) microstructures of the alloys: (e) Nb-12Si-5Mo, and (f) Nb-12Si-5Mo-20Ti [29, 30].

The compression tests carried out at a strain rate of 10^{-3} s^{-1} between 900°C and 1100°C have shown that Ti addition does not affect the compressive strength significantly, with the exception of a modest increase being observed in the alloy with hypoeutectic composition at temperatures $\geq 1000 \text{ }^\circ\text{C}$ (Fig. 14(a-b)) [32]. At a given temperature, the alloys with hypoeutectic composition have been found to possess much superior strength retention ($\sigma_{0.2}(\text{T})/\sigma_{0.2}(\text{RT})$) as a fraction of the yield strength at room temperature, being promoted by solid solution strengthening of the Nb_{ss} by Mo or Mo+Ti (Fig. 14(c-d)). The addition of Ti has been found to have led to improved high temperature strength retention, with the contribution being most strongly noticed for the hypoeutectic composition at 1100 °C.

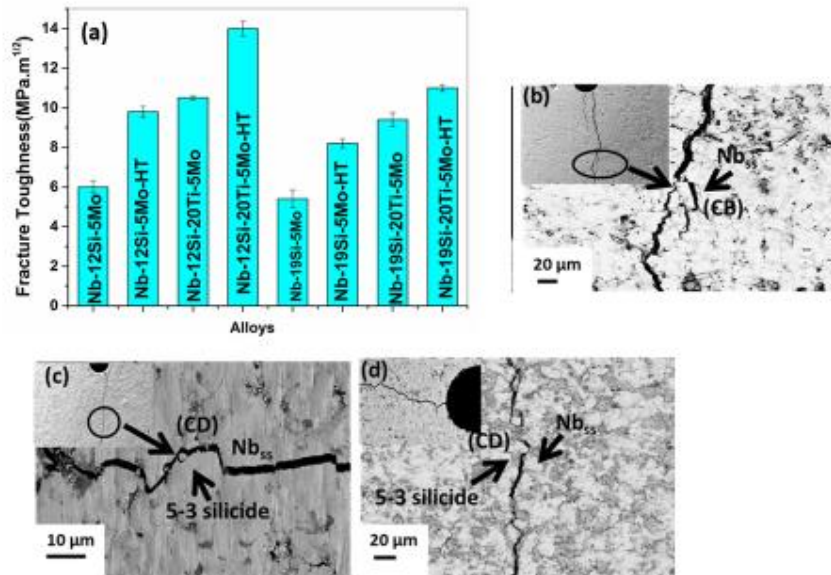


Fig. 13 (a) Bar-charts depicting the fracture toughness of Nb-Si-Mo and Nb-Si-Mo-Ti alloys (HT indicates “annealed at 1500 °C for 100 h); (b-d) SEM images of the crack profiles showing the interaction of the propagating crack with the microstructure [31].

Non-isothermal oxidation tests by heating up to 1300 °C and isothermal oxidation tests carried out in the range of 900-1200 °C (Fig. 15(a)) have shown lower mass gain for the Ti-containing alloys, compared to that observed in the corresponding hypoeutectic or hypereutectic ternary Nb-Si-Mo alloy [32]. Additionally, the alloys with hypereutectic composition have exhibited superior oxidation resistance compared to the corresponding hypoeutectic alloys. The products of oxidation include Nb₂O₅ and SiO₂, with TiO₂, TiNb₂O₇ and Ti₂Nb₁₀O₂₉ being formed additionally in the oxide scales of the Nb-12Si-5Mo-20Ti and Nb-19Si-5Mo-20Ti alloys (Fig. 15(b)). Further, the thickness of oxide scales is found to be lower in case of the Ti containing alloys having either hypoeutectic or hypereutectic composition (Fig 15(c-d)). Analysis of the oxidation kinetics suggest an initial phase of interface-reaction controlled rapid increase of mass, followed by the stage of parabolic behavior, where diffusion of O²⁻ or Ti⁴⁺ through the oxide scale appears to be the rate-controlling in ternary or Ti-containing quaternary alloys, respectively. The formation of a relatively defect-free oxide scale, along with reduced oxygen solubility and diffusivity due to the presence of Mo and Ti in Nb_{ss}, along with formation of SiO₂-rich oxide on Nb-19Si-5Mo-20Ti alloy at 1100 °C and 1200 °C appear to be responsible for its superior oxidation resistance.

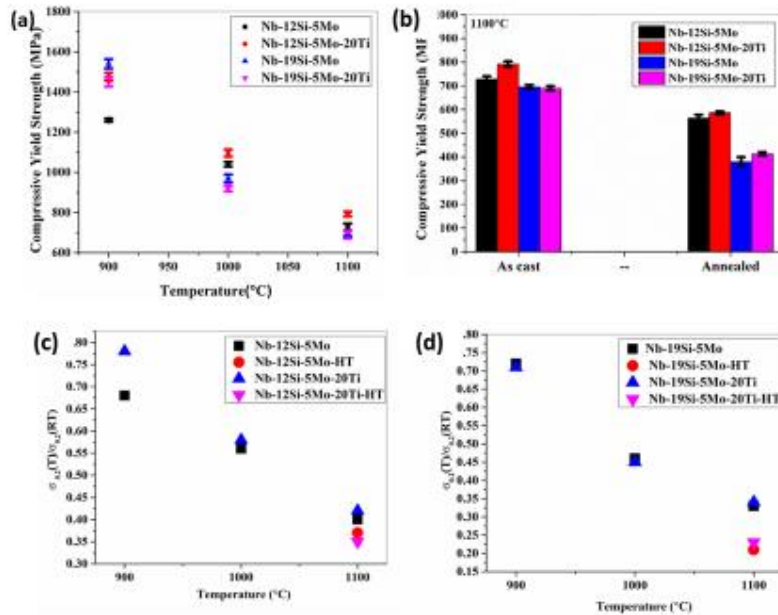


Fig. 14. Results of compression tests carried out at the strain rate of 10^{-3} s^{-1} on the Nb-Si-Mo and Nb-Si-Mo-Ti alloys [31]: (a) Plots depicting the variation of compressive yield strength with temperature, (b) Bar-charts depicting compressive yield strengths of arc-melted and annealed alloys; as well as plots showing the variation of high temperature strength retention as function of temperature for (c) arc-melted and (d) annealed samples.

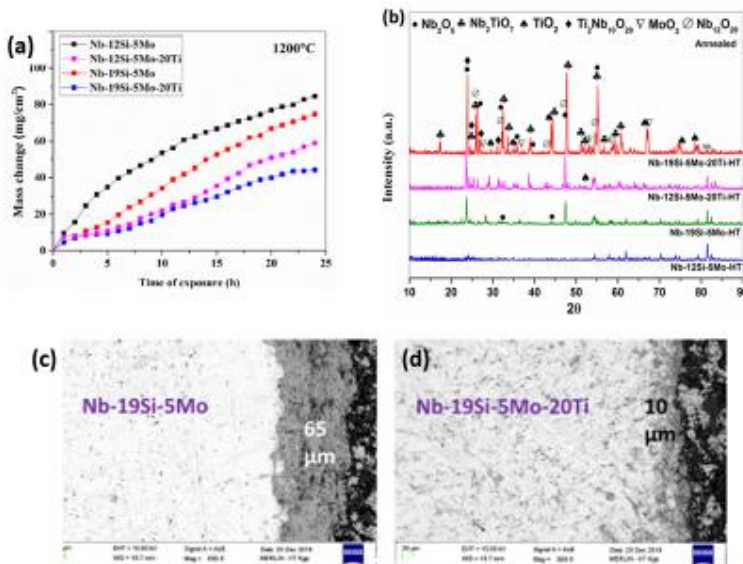


Fig. 15. Results of isothermal oxidation tests [32]: (a) Plots showing the variation of mass gain with temperature; (b) Typical XRD pattern from the oxide scale formed at

1100 °C, as well as SEM images depicting the cross-sections of the oxide scales formed at 1100 °C on the alloys with compositions: (c) Nb-19Si-5Mo, and (d) Nb-19Si-5Mo-20Ti.

2.4 Development of ultra-high temperature ceramics

The ultra-high temperature ceramics based on ZrB_2 and HfB_2 have recently received major attention for use in leading edges and nose cones of hypersonic vehicles, because of their high melting points, moderate thermal and electrical conductivity, low coefficient of thermal expansion, and high chemical inertness in typically extreme environments. It has been reported in an earlier study that the oxidation of ZrB_2 is initiated at $\sim 800^\circ\text{C}$ leading to the formation of a mixture of ZrO_2 and B_2O_3 (l) on the outermost surface as the oxidation products [33]. Since the ZrO_2 is an anion deficient semiconductor, the diffusion of oxygen anions is found to be very high through it [34]. The oxidation resistance of ZrB_2 is significantly improved by reinforcing with SiC, which leads to the formation of a protective scale of borosilicate glass.

The densification of ZrB_2 is quite challenging due to low ionic diffusivity, presence of oxide impurities at powder particle surfaces, along with the requirement of high temperature for densification, which in turn leads to coarsening. Pressureless sintering of ZrB_2 -SiC composites has been found to lead to complete densification with the help of suitable additives. This process is considered promising for preparing near-net shaped composites, but needs to be optimized to maximize the amount of densification without grain coarsening, such that desirable mechanical properties are achieved. On the other hand, hot pressing leads to near-theoretical density with impressive mechanical properties, but this process is suitable only for fabrication of simple shapes. Additionally, spark plasma sintering can be used for densification at relatively lower temperatures without grain coarsening.

2.4.1. Pressureless sintered ZrB_2 -SiC composites

In my research group, a technique for pressureless sintering of ZrB_2 -SiC composites has been developed by using B_4C and C (added as 2 wt% phenolic resin) as additives [35]. In this process, the composite mixture prepared by blending of powders and additives in a ball mill with WC-Co vials and balls, is cold compacted in a uniaxial press, and subsequently pressureless sintered in argon environment. This process involves pre-sintering at 850°C for 1 h to get rid of volatile constituents of phenolic resin such that only C is left behind. Thereafter, the powder mixture is subjected to intermediate holds at 1250°C and 1600°C for 0.5 h each for the surface oxides to be reduced by B_4C and C, and then finally sintered at 2000°C for 1 h. The temperatures for intermediate hold have been chosen such that the free energies of the

reactions leading to the reduction of SiO_2 , B_2O_3 and ZrO_2 by B_4C or C are negative [36]. Observation of the microstructures has shown a W-rich network at ZrB_2 grain boundaries and ZrB_2 -SiC interfaces (Fig. 16(a-b)). The W is considered to have been added to the powder mixture during ball-milling by erosion of WC-Co balls and vials by the abrasive SiC particles, which is supported by increase of W concentration with SiC content. The formation of a continuous network along with the rounded corners of grains is considered as the evidence for the formation of a liquid phase, which appears to have aided densification. The relative density of the pressureless sintered composites is found to scale with SiC content, and also increase significantly on subjecting to isothermal hold at 1250 °C and 1600 °C for 0.5 h (Fig. 16(c)) [35].

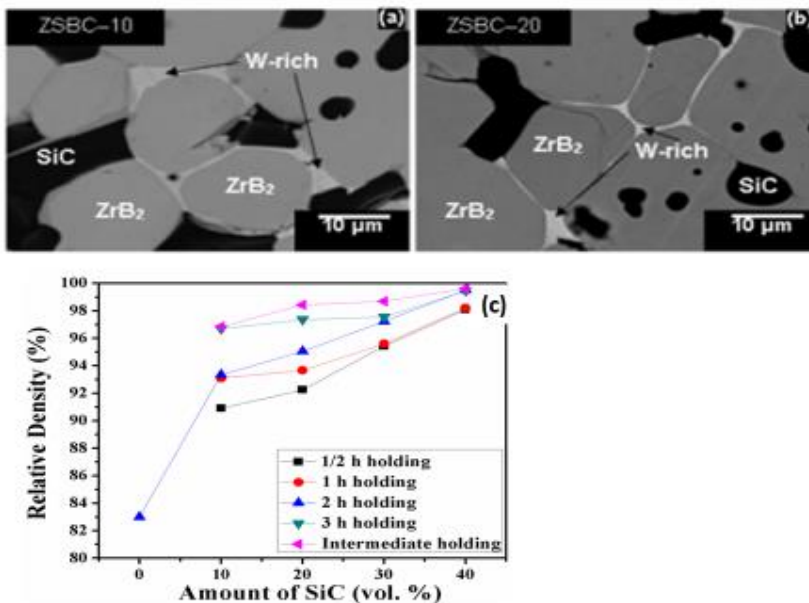


Fig. 16 SEM (BSE) images depicting the microstructures of pressureless sintered ZrB_2 -SiC composites with SiC content of (a) 10 vol%, (b) 20 vol% (with W-rich phase at the interfaces), and (c) plots of relative density against SiC content for different sintering durations [35].

The thermal diffusivity of the investigated composites measured by the laser flash method, has been found to be the highest for the ZrB_2 -20 vol% SiC composite (Fig. 17(a)) [37]. Although the thermal conductivity of SiC is higher than that of ZrB_2 , reduction in grain size along with the increase in interfacial area with increase in SiC volume fraction leads to enhanced phonon scattering, which in turn lowers the thermal conductivity for SiC content >20 vol%. Among the samples subjected to thermal shock by heating the to 800 °C, 1000 °C and 1200 °C followed by quenching in water has shown the least increase in indentation crack length as well as the lowest reduction of hardness for the ZrB_2 -20 vol% SiC composite (Fig. 17(b-c)). Such an observation

indicating the lowest thermal shock induced damage in the ZrB₂-20 vol% SiC composite is ascribed to its thermal conductivity found to be the highest.

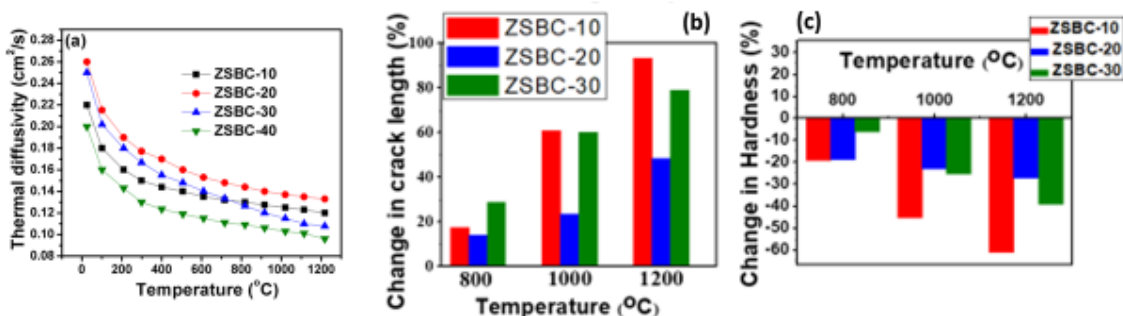


Fig. 17 (a) Plots depicting the variation of thermal diffusivity with increasing temperature; as well as bar charts showing changes in (b) indentation crack length and (c) hardness measured using Vickers hardness testing machine operated at the load of 10 kgf [37].

The samples subjected to ablation tests by exposing to oxy-acetylene (OA) flame have shown the average temperatures at front face and back face as ~2200 °C and ~1600 °C, respectively with variations of ± 50 °C [37]. The slope for rise of temperature has been found to be the sharpest in case of the ZrB₂-20 vol.% SiC composite, probably because of its higher thermal conductivity. On exposure to the OA flame, the surfaces of composites with 10 or 30 vol% SiC appear to be rough with a network of pores with significantly large discontinuities, whereas the surface of the ZrB₂-20 vol% SiC composite has been found to be comparatively smooth with finer pores (Fig. 18(a-f)). The EDS spectrum of the ablated surfaces (Fig. 18(g)) has shown peaks of Zr, Si and O, indicating the formation of ZrO₂ and ZrSiO₄ as confirmed by the XRD analysis as well (Fig. 18(h)). As indicated by the ZrO₂-SiO₂ phase diagram, ZrO₂ + liquid is formed at the OA flame temperature, which on solidification forms ZrO₂ + ZrSiO₄ [38]. The ZrO₂ acts as thermal insulation for the composite, whereas the liquid closes the surface pores. As is evident from the bar-charts depicting the changes in Young's modulus due to the ablation test (Fig. 18(h)), the ZrB₂-20 vol% SiC composite has been found to be more resistant to damage compared to that with 10 vol% SiC composite is probably due to the less amount of liquid formed in the latter composite at the flame temperature in case of the latter composite. Having higher than 20 vol% SiC is found to be detrimental probably because of the active oxidation of SiC to form SiO(g) becoming predominant. Formation of ZrSiO₄ lowers the formation of SiO (g). The amount of ZrSiO₄ is found to be maximum in the oxide scale of ZrB₂-20 vol% SiC composite, because an optimum amount of ZrO₂ and SiO₂ are probably formed during high temperature exposure.

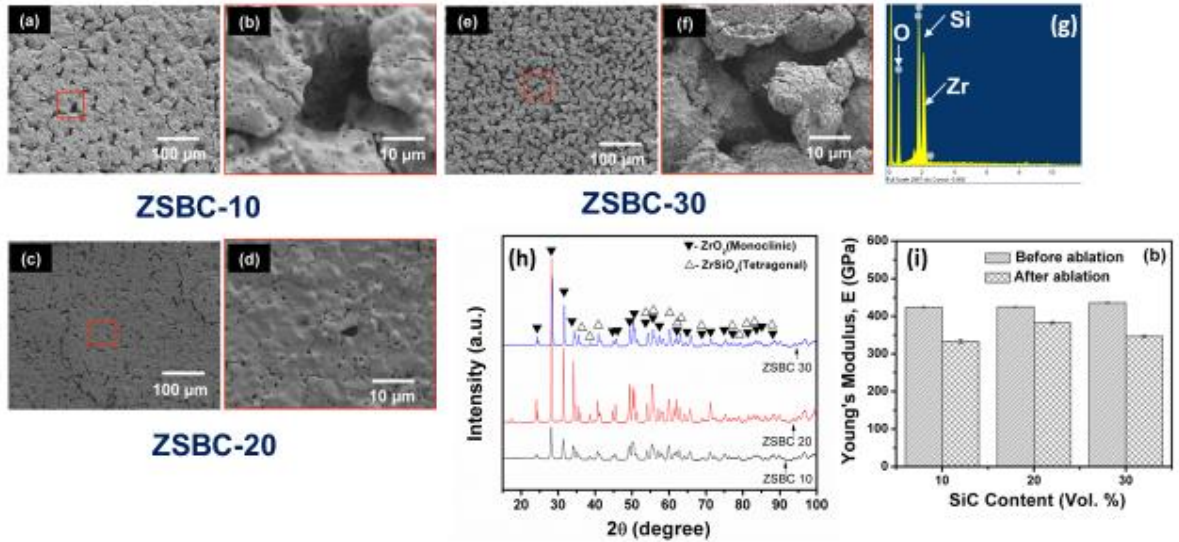


Fig. 18. Results of ablation tests [37]: SEM images depicting the top surfaces of the oxide scales formed as a result of ablation test on (a-b) $\text{ZrB}_2\text{-20SiC-7LaB}_6$ (ZSBCL-7); (c-d) $\text{ZrB}_2\text{-20SiC-10LaB}_6$ (ZSBCL-10); (e-f) $\text{ZrB}_2\text{-20SiC-14LaB}_6$ (ZSBCL-14); (g) EDS spectrum from the oxide scale showing peaks of Zr, Si and O; as well as (h) XRD patterns from the oxide scales; and (i) bar charts depicting Young's modulus before and after ablation test.

2.4.2. Hot pressed $\text{ZrB}_2\text{-SiC}$ composite

Hot pressing in argon environment at 2000 °C under 30 MPa pressure for 30 min was used to process composites having the compositions of $\text{ZrB}_2\text{-20 vol% SiC}$, $\text{ZrB}_2\text{-20 vol% SiC-5 vol% Si}_3\text{N}_4$, and $\text{ZrB}_2\text{-20 vol% ZrC-20 vol% SiC-5 vol% Si}_3\text{N}_4$ [39]. A typical microstructure of the hot-pressed $\text{ZrB}_2\text{-20 vol% SiC}$ composite is shown in Fig. 19(a). Evaluation of the room temperature mechanical properties these composites has shown that the $\text{ZrB}_2\text{-20 vol% SiC-5 vol% Si}_3\text{N}_4$ composite possesses the highest hardness ($\sim 21.2 \pm 2$ GPa), flexural strength ($\sim 520 \pm 6$ MPa) and fracture toughness ($\sim 7.8 \pm 0.6$ MPa $\sqrt{\text{m}}$) among the investigated hot-pressed composites. The $\text{ZrB}_2\text{-20 vol% SiC}$ composite processed by hot pressing has been found to possess finer grain size and higher hardness compared to that obtained by pressureless sintering.

The creep tests carried out in the temperature range of 1300-1425 °C on $\text{ZrB}_2\text{-20 vol% SiC}$ (ZS) and $\text{ZrB}_2\text{-20 vol% SiC-5Si}_3\text{N}_4$ (ZSS) composites have consistently shown lower steady state strain rate in case of the former composite (Fig. 19(b)) [40]. The stress exponent (n) has been found to be between 1.1 and 1.7 for the ZS, and

between 0.6 and 1.6 for the ZSS, with the values being <1 for temperatures ≥ 1400 °C (Fig. 19(b)). The obtained values of n are suggestive of diffusion controlled creep. The activation energy has been found as $\sim 95 \pm 32$ kJ/mol at temperatures ≤ 1350 °C, which is close to that for diffusivity of O^{2-} through SiO_2 , as shown in Fig. 19(c) and (d). On the other hand, the activation energy at temperatures ≥ 1350 °C has been found as $\sim 470 \pm 20$ kJ/mol, which agrees with that required for the viscoplastic flow of the intergranular glassy film. The values of $n < 1$ observed for the ZSS composite creep tested at ≥ 1400 °C is ascribed to the presence of Si_3N_4 in its microstructure, which is known to undergo by grain boundary sliding accommodated by solution and reprecipitation. At high temperature, the Si_3N_4 dissolves in the Si-N-O glassy phase, followed by precipitation of the Si_2N_2O at the grain boundaries and particle-matrix interfaces. Additionally, the post-creep microstructures have shown cracks at ZrB_2 grain boundaries and ZrB_2 -SiC interfaces, along with voids at grain boundary triple points, which appear to have formed by grain boundary sliding, as shown in Fig. 19(e).

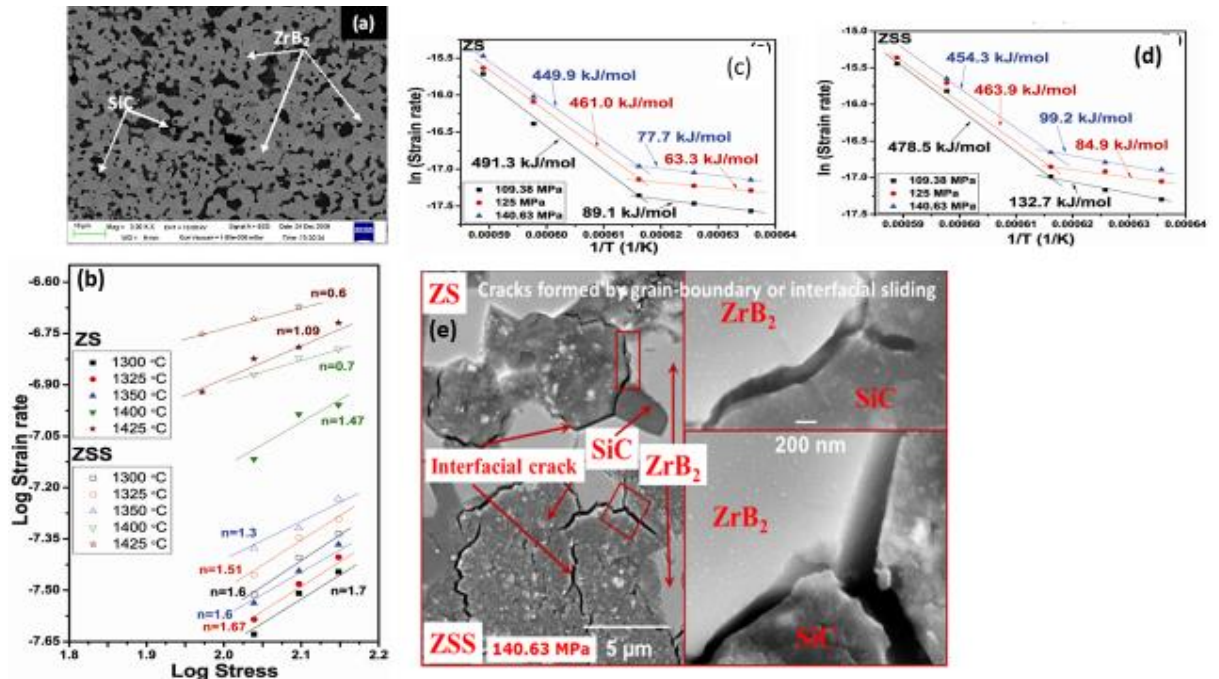


Fig. 19 (a) SEM image showing the microstructure of the ZrB_2 -20 vol% SiC composite, (b) log-log plots of steady state creep strain rate with stress with best-fit lines drawn to find stress exponents (n), Plots of log creep strain rate against the reciprocal of absolute temperature to find activation energy for creep for the composites (c) ZrB_2 -20 SiC (ZS) and (d) ZrB_2 -20 SiC-5 Si_3N_4 (ZSS), as well as (e) SEM images showing evidence of cracking due sliding of grain boundaries and ZrB_2 -SiC interfaces during creep [40].

2.4.3. Composites processed by spark plasma sintering

2.4.3.1 Processing

The ZrB₂-20 vol% SiC composites with 7, 10 and 14 vol% LaB₆ (marked as ZSBCL7, ZSBCL10 and ZSBCL14, respectively) added at the expense of ZrB₂ along with B₄C and C being present as additives, have been processed by spark plasma sintering at 1600 °C or 1800 °C in argon environment using ram pressure of 50 and 70 MPa, respectively [41]. For SPS at 1600 °C and 1800 °C, the samples were isothermally held at 1300 °C and 1500 °C, respectively for 2 min. In spite of higher temperature and pressure, the densification achieved is less at 1800 °C compared to that at 1600 °C. The spark plasma sintering process can be divided into three zones (Fig. 20(a-b)). The first zone includes the stage of heating to the intermediate hold temperature, whereas in the second zone the temperature is raised to that of intermediate hold. In the third zone, soaking has been carried out at 1600 °C or 1800 °C for the maximum relative density to be achieved (Fig. 20(c)). The relative densities prior to soaking in the third zone are ~92-94% for SPS at 1600 °C, and ~84-89% for SPS at 1800 °C. Based on the analysis of the ram displacement the densification rates at 1600 and 1800 °C have been calculated, and the creep occurring during soaking at 1600 °C and 1800 °C has been analysed to find stress exponents (n), 4.9-6.7 and 2-3.2, respectively, as shown in Fig. 20(d) and (e), respectively. Based on the values of n, the mechanism of creep is identified as dislocation climb controlled for SPS at 1600 °C. On the other hand, the values of n for SPS at 1800 °C suggest the predominance of diffusion controlled creep with grain boundary sliding in case of ZSBCL-7 and ZSBCL-10, but the operation of dislocation glide controlled creep for the ZSBCL-14. Arrays of dislocations (straight and curved) with some having jogs in the ZrB₂ grains can be considered as the evidence of dislocation creep (Fig. 20(f)). Lower densification during SPS at 1800 °C is ascribed to incomplete removal of impurity oxides along with higher rate of vaporization of B₂O₃, which leads to the retention of porosities.

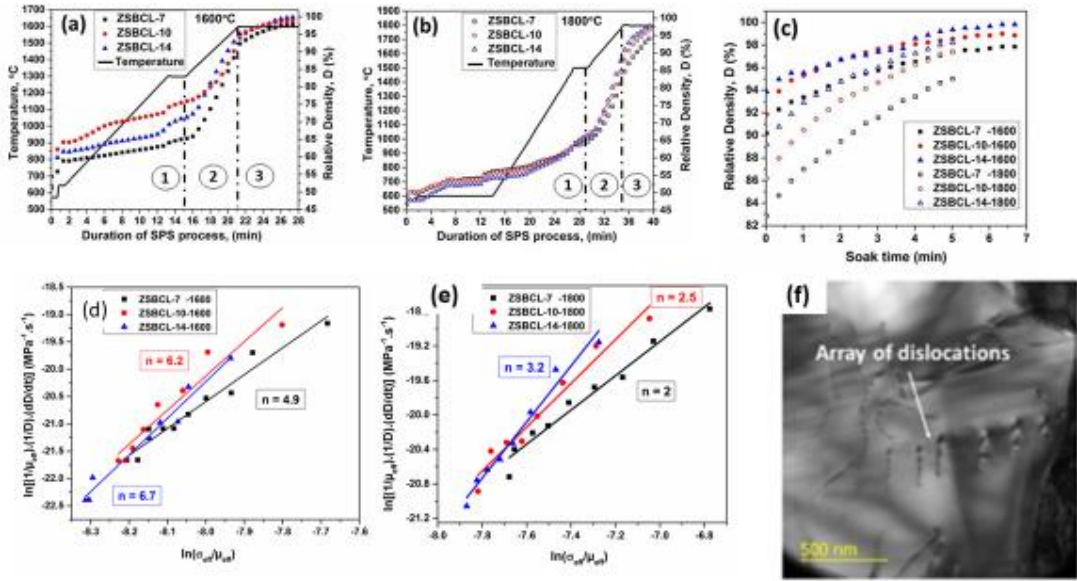


Fig. 20 Plots depicting the variation of temperature for spark plasma sintering at (a) 1600 °C, and (b) 1800 °C; (c) plots showing the variation of relative density with duration of soaking; plots of densification rate with normalized stress for final soaking at (d) 1600 °C and (e) 1800 °C; as well as (f) a TEM bright field image showing dislocation activity in the ZrB₂-20 vol% SiC-10 LaB₆ composite [41]

2.4.3.2 Oxidation behaviour

Non-isothermal oxidation experiments carried out by heating in a thermogravimetric analyser in air from room temperature to 1400 °C have shown the highest mass gain for the ZSBCL-14 composites, which is ascribed to rapid oxidation of the LaB₆ [42] However, isothermal and cyclic oxidation experiments for 24 h in the range of 1300-1500 °C have shown the least mass gain in case of the ZSBCL-14 composite, which is ascribed to the formation of a protective scale after exposure for a minimum duration of 8-10 h.

On isothermal oxidation at 1300 °C, the change in mass gain with time follows a parabolic behaviour with a protective layer of BSG being developed right after the outermost layer of La₂Si₂O₇ (Fig. 21(a-c)) [43]. The contribution of LaB₆ to the oxide scale formation includes the formation of B₂O₃ along with La₂O₃, which combines with SiO₂ and oxygen at the outer surface to form La₂Si₂O₇. It should be also noted that the amount of B₂O₃ formed by the oxidation of one of LaB₆ is 3 times more than that produced by the oxidation of a mole of ZrB₂. Therefore, the growth rate of BSG is found to increase following a linear relation with the LaB₆ content of the

investigated composites during exposure up to 8 h, but decrease with LaB_6 content during 8-24 h (Fig. 21(d-e)). For durations of both 0-8 h and 8-24 h, the parabolic rate constant, k_p has been found to decrease with the increasing LaB_6 content, which can be considered as a confirmation of the critical role played by the BSG layer in protection against oxidation (Fig. 21(f-g)).

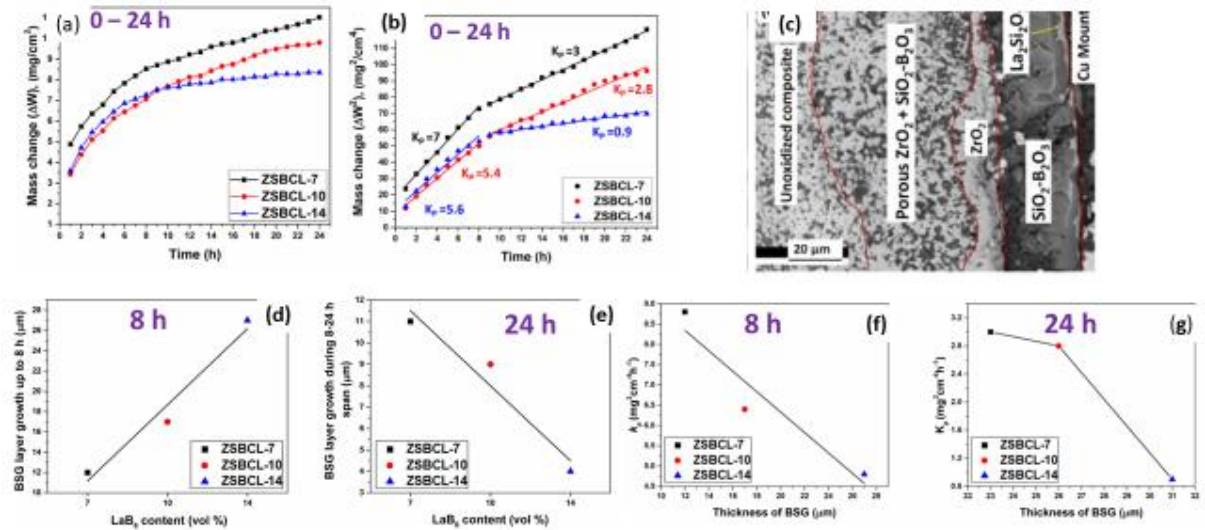


Fig. 21. The results of oxidation tests at 1300 °C [43]: (a) plots of mass change with temperature during isothermal exposure at 1300 °C; (b) plots depicting the variation of (mass gain per unit area)² with time to find parabolic rate constant, k_p ; (c) SEM (BSE) image depicting the oxide scale cross-section formed after exposure for 24 h in the ZrB₂-20 SiC-14 LaB₆ composite; plots depicting the variation of borosilicate glass (BSG) layer growth rate with LaB₆ content for durations up to (d) 8 h, and (e) 24 h; as well as the plots showing variation of k_p with thickness of BSG for durations up to (f) 8 h, and (g) 24 h.

Isothermal exposure for 24 h at 1400 and 1500 °C has led to formation of oxide scales containing an outer layer of BSG with a thin film of $\text{La}_2\text{Si}_2\text{O}_7$ on the top surface, which is followed by the layers comprising coarse ZrO_2 +BSG, fine ZrO_2 + BSG, followed by a SiC depleted layer at the composite-oxide interface (Fig. 22) [42,44]. In the oxide scale of the composite isothermally exposed at 1500 °C, a mixed layer containing La-Zr-Si-B-O is present above the SiC depleted layer. The SiC depleted layer is believed to have formed by the active oxidation of SiC, leading to the formation and escape of SiO (g) and CO (g). Higher active oxidation of SiC at 1500 °C than that at 1400 °C is also considered to be responsible for lower mass gain observed at the higher temperature. The BSG containing B_2O_3 (l) formed at the oxide-composite interface by oxidation of ZrB₂ and LaB₆ is considered to have enough fluidity for moving outwardly by capillary action, filling up the pores and thereby

form the outermost layer of the oxide scale. The formation of an inner layer enriched in La-Zr-Si-B-O within the oxide scale on exposure at 1500 °C indicates that ZrO_2 and La_2O_3 formed by oxidation of ZrB_2 and LaB_6 , respectively are partially dissolved in the BSG. Of course, its viscosity is increased by dissolution of ZrO_2 and La_2O_3 , along with stabilization of the glass network. The $ZrO_2 + BSG$ layer is expected to have formed by the precipitation of ZrO_2 from the BSG. Additionally, the outermost layer of $La_2Si_2O_7$ is also considered to have formed by precipitation from the BSG. The activation energy for oxidation obtained on the basis of the k_p values obtained by analyzing the isothermal exposure test data is found to be considerably greater than that of O^{2-} required for diffusion through SiO_2 , because of the complex nature of the BSG scale containing ZrO_2 and La_2O_3 , formed on the investigated composites.

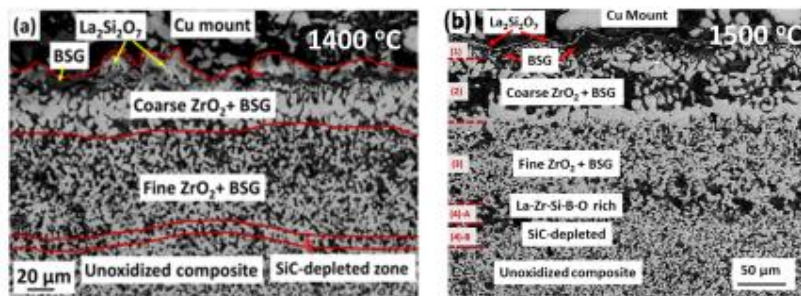


Fig. 22. SEM (BSE) images showing various layers of oxide scales formed during isothermal exposure for 24 h at (a) 1400 °C and (b) 1500 °C [42, 44].

Cyclic oxidation behaviour has been studied by subjecting 24 cycles of 1 h exposure (24 h) and 10 cycles of 10 h exposure (100 h) at 1400 °C [42]. The oxide scale formed by cyclic exposure has been found to contain an outer compact layer (OCL) comprising BSG+ $ZrSiO_4$ with a film of $La_2Si_2O_7$ at the top surface, which is followed by an intermediate layer of ZrO_2+BSG , and thereafter a SiC-depleted zone located at the oxide-composite interface (Fig. 23(a)). After cyclic oxidation for 24 h, the mass gain is found to be the least value in the ZSBCL-10, whereas after 100 h of cyclic oxidation, the ZSBCL-14 is found to have gained the least mass, with ZSBCL-7 being the most prone to oxidation under either conditions of cyclic oxidation (Fig. 23(b-c)). The values of k_p are found to decrease following a linear relationship with increase in the thickness of the OCL in the oxide scales of the composites subjected to 10 cycles of 10 h each at 1400 °C (Fig. 23(d)). This observation can be considered as a confirmation of the role of the OCL in protection against oxidation.

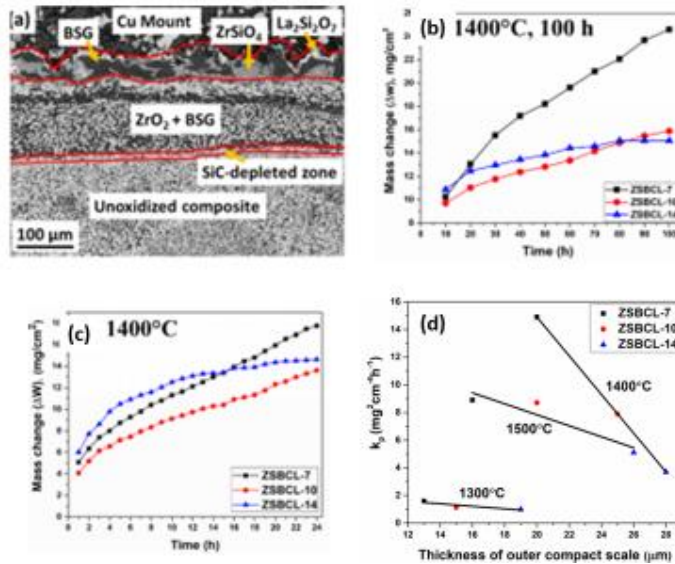


Fig. 23 (a) SEM BSE image depicting the oxide scale formed by cyclic exposure at 1400 °C for 100 h (10 cycles of 10 h each) on ZrB_2 -20Si-14 LaB_6 composite; as well as plots depicting variation of mass gain per unit area with duration for (b) 24 cycles of 1 h exposure (24 h); (c) 10 cycles of 10 h exposure (100 h); as well as (d) variation of parabolic rate constant (k_p) with thickness of the outer compact layer in the oxide scale in (a) [42].

3. Concluding remarks and future directions

The research outcomes discussed in this lecture may be summarized as follows:

- (1) Mushy state rolling with prior cold rolling has been found to significantly improve creep resistance of in-situ $Al_4.5Cu-5TiB_2$ composite.
- (2) A steady state behaviour in tertiary creep stage of IN617 alloy caused by carbide precipitation slows creep damage at 750-800 °C.
- (3) Creep resistance of single Ni-based superalloy is much more along $\langle 100 \rangle$ than that along $\langle 110 \rangle$. Coarsening of γ' is preferred along $\langle 100 \rangle$ irrespective of stress axis orientation.
- (4) The Mo-Si-B alloys exhibit impressive strength retention and oxidation resistance till 1300°C. Minor Zr addition improves oxidation resistance in both dry and moist air.
- (5) High temperature strength and oxidation resistance, along with fracture toughness of hypo and hypereutectic Nb-Si-Mo alloys are significantly enhanced on Ti addition.

(6) Reinforcing with 20 vol% SiC is found optimum for ZrB₂ based UHTCs. The creep involves grain boundary sliding accommodated by diffusion. The oxidation resistance is noticeably improved through LaB₆ addition.

Whereas incremental research is in progress on metal matrix composites and Ni-based superalloys for further improvement, a significant leap forward is required for Mo and Nb-silicides to come in to practical use, considering the limitations of fabrication and limited room temperature fracture toughness. It is quite a challenge to balance the contradictory requirements of room temperature toughening with high temperature oxidation resistance and strength retention. Silicide coatings applied by pack cementation on the Nb-Si based alloys have yielded promising results. Further, the observation of improved mechanical properties and oxidation resistance with Mo+Ti addition to the Nb-Si based alloys is promising. There has been an effort recently by the researchers to fabricate the ZrB₂-based UHTCs with continuous C-fibre reinforcement, which has led to superior damage tolerant behaviour.

Acknowledgements

The present lecture is based on the results obtained in course of dissertation research by the present and former students, Dr. Monalisa Mandal, Mr. Sumanta Bagui, Mr. Dibyendu Chakraborty, Mr. Arvind Srivastava, Dr. Sharma Paswan, Dr. Nandkishor Kumar, Dr. Kausik Chattopadhyay, Ms. Kasturi Sala, Dr. Manab Mallik, Mr. Sabyasachi Roy and Mr. Sunil Kashyap. Sincere thanks are also due to the technical staff of the Central Research Facility and various department laboratories for help and support, whenever required. The financial support of Defence Research and Development for sponsoring some of the research is gratefully acknowledged.

References

1. A. Mandal, R. Maiti, M. Chakraborty, and B.S. Murty, "Effect of TiB₂ particles on aging response of Al-4Cu alloy," *Mater. Sci. Eng. A*, vol. 386, pp. 296–300 (2004).
2. Mervin A. Herbert, Chandan Sarkar, R. Mitra and M. Chakraborty, "Microstructural evolution, hardness and alligating in the mushy state rolled cast Al-4.5Cu alloy and in-situ Al_{4.5}Cu-5TiB₂ composite," *Metall. Mater. Trans. A*, vol. 38(9), pp. 2110-2126 (2007).
3. A. Jana, I.G. Siddhalingeswar, and R. Mitra, "Effect of homogeneity of particle distribution on tensile crack propagation in mushy state rolled in-situ Al-4.5Cu-5TiB₂ particulate composite," *Mater. Sci. Eng. A.*, vol. 575, pp. 104-110 (2013).

4. Monalisa Mandal and Rahul Mitra, "Effect of pre-cold rolling on the evolution of microstructure, microtexture, and mechanical properties of the mushy state rolled in-situ Al-4.5Cu-5TiB₂ composite," *Mater. Char.*, vol. 146, pp. 267-278 (2018).
5. Monalisa Mandal and Rahul Mitra, "Effect of microstructure and microtexture evolution on creep behavior of hot-rolled and mushy-state rolled Al-4.5Cu-5TiB₂ in-situ composite," *Mater. Sci. Eng. A*, vol. 760, pp. 88-104 (2019).
6. Sumanta Bagui, Bibhu Prasad Sahu, Kinkar Laha, Soumitra Tarafder and Rahul Mitra, "Creep deformation behavior of Inconel 617 alloy in the temperature range of 650 - 800 °C," *Metall. Mater. Trans. A*, vol. 52, pp. 94-107 (2021)
7. D. Chatterjee, N. Hajari, N. Das, and R. Mitra, "Microstructure and creep behavior of DMS4-type nickel based superalloy single crystals with orientations near <001> and <011>," *Mater. Sci. Eng. A.*, vol. 528, pp 604-613 (2010).
8. R. Mitra, "Mechanical Behavior and Oxidation Resistance of Structural Silicides," *Inter. Mater. Rev.*, vol. 51(1), pp. 13-64 (2006).
9. T. B. Massalski, H. Okamoto, P. R. Subramanian and L. Kacprzak (eds.): 'Binary alloy phase diagrams', Vol. 2, 1333, 1631, 2054; 1987, Materials Park, OH, ASM.
10. R. Mitra, V. V. Rama Rao and A. Venugopal Rao, "Effect of small Al alloying on microstructure and mechanical properties of molybdenum disilicide," *Intermetallics*, vol. 7(2), pp. 213-232 (1999).
11. R. Mitra and A. Venugopal Rao, "Effect of processing methods on purity and structure of internal interfaces and high temperature strength of MoSi₂ and MoSi₂-SiC composites," *Trans. Ind. Ceram. Soc.*, vol. 60(1), pp. 12-20 (2001).
12. H. Nowotny, E. Dimakopoulou and H. Kudielka, *Monatsh. Chem.*, vol. 88, 180 (1957).
13. R. Mitra, "Silicides and Silicide Matrix Composites for High Temperature Structural Applications," in *Handbook of advanced ceramics and composites*, edited by Yashwant R. Mahajan and Roy Johnson, Springer Nature Switzerland AG 2019, pp. 1-55 (2019) https://doi.org/10.1007/978-3-319-73255-8_40-1
14. M.K. Meyer, M.J. Kramer, and M. Akinc, "Oxidation behavior of boron-modified Mo₅Si₃ at 800 -1300 C," *Intermetallics*, vol. 4, pp. 273–81 (1996).
15. T. Hayashi, K. Ito, K. Ihara, M. Fujikura and M. Yamaguchi, "Creep of single crystalline and polycrystalline T2 phase in the Mo–Si–B system," *Intermetallics*, 12(7–9), 699-704 (2004).

16. R. Mitra, A.K. Srivastava, N. Eswara Prasad, and Sweety Kumari, "Microstructure and Mechanical Behaviour of Reaction Hot Pressed Multiphase Mo-Si-B and Mo-Si-B-Al Intermetallic Alloys," *Intermetallics*, vol. 14(12), pp. 1461-1471 (2006).
17. R. Mitra, K. Chattopadhyay, A.K. Srivastava, K.K. Ray, and N. Eswara Prasad, "Effect of Ductile and Brittle Phases on Deformation and Fracture Behaviour of Molybdenum and Niobium Silicide Based Composites," *Key Eng. Mater.*, vol. 395, pp. 179-192 (2009).
18. Sharma Paswan, R. Mitra and S.K. Roy, "Oxidation Behaviour of the Mo-Si-B and Mo-Si-B-Al Alloys in the Temperature Range of 700-1300°C," *Intermetallics*, Vol. 15, pp. 1217-1227 (2007).
19. Barna Roy, J. Das and R. Mitra, "Transient stage oxidation behavior of $\text{Mo}_{76}\text{Si}_{14}\text{B}_{10}$ alloy at 1150 °C" *Corr. Sci.*, vol. 68, pp. 231-237 (2013).
20. N. K. Kumar, J. Das, and R. Mitra, "Effect of Zr addition on microstructure, hardness and oxidation behavior of arc-melted and spark plasma sintered multiphase Mo-Si-B alloys," *Metall. Mater. Trans. A.*, vol. 50A, pp. 2041-2060 (2019).
21. N.K. Kumar, J. Das and R. Mitra, "Effect of moist air and minor Zr addition on oxidation behavior of arc-melted multiphase Mo-Si-B alloys in the temperature range of 1000°C-1300°C," *Oxid. Met.*, vol. 93, pp. 483-513 (2020).
22. M. E. Schlesinger, H. Okamoto, A. B. Gokhale and R. Abbaschian, "The niobium-silicon (Nb-Si) system," *J. Phase Equil.*, vol.14 (4), 502-509 (1993).
23. W.Y. Kim, H. Tanaka, A. Kasama, R. Tanaka, and S. Hanada, "Microstructure and room temperature deformation of Nb_{ss}/Nb₅Si₃ in situ composites alloyed with Mo," *Intermetallics*, vol. 9, pp. 521-27 (2001).
24. W. Li, H. Yang, A. Shan, L. Zhang, and J. Wu, "Effect of Mo addition on the phase stability of β -Nb₅Si₃ phase," *Intermetallics*, vol. 14, pp. 392-95 (2006).
25. K. Chattopadhyay, R Sinha, R. Mitra, and K.K. Ray, "Effect of Mo and Si on morphology and volume fraction of eutectic in Nb-Si-Mo alloys," *Mater. Sci. Eng. A.*, vol. 456, pp. 358-363 (2007).
26. K. Chattopadhyay, G. Balachandran, R. Mitra, and K.K. Ray, "Effect of Mo on Microstructure and Mechanical Behaviour of Cast Nb_{ss}-Nb₅Si₃ In-Situ Composites," *Intermetallics*, Vol. 14(12), pp. 1452-1460 (2006).
27. K. Chattopadhyay, Structure-Property Relationships in Nb-Si-Mo alloys, PhD dissertation, IIT Kharagpur (2008).
28. K. Chattopadhyay, R. Mitra, and K.K. Ray, "Non-isothermal and Isothermal Oxidation Behaviour of the Nb-Si-Mo Alloys," *Metall. Mater. Trans. A.*, vol. 39A, pp. 577-592 (2008).

29. Kasturi Sala, Swapnil A. Morankar, and Rahul Mitra, "Effect of Ti or Fe addition and annealing on microstructural evolution and mechanical properties of hypereutectic Nb-Si-Mo alloys," *Metall. Mater. Trans. A*, vol. 52, pp. 1185-1211 (2021).
30. Kasturi Sala and Rahul Mitra, "Microstructural evolution and mechanical properties of as-cast and annealed Nb-Si-Mo based hypoeutectic alloys with quaternary additions of Ti or Fe", *Mater. Sci. Eng. A*, vol. 802, 140663 (2021).
31. Kasturi Sala and Rahul Mitra, "Effect of Ti addition and microstructural evolution on toughening and strengthening behavior of as cast or annealed Nb-Si-Mo based hypoeutectic and hypereutectic alloys," *Metall. Mater. Trans. A*, Vol. 52, pp. 3436-59 (2021).
32. Kasturi Sala, Sunil Kashyap and Rahul Mitra, "Effect of Ti addition on the kinetics and mechanism of non-isothermal and isothermal oxidation of Nb-Si-Mo alloys at 900 °C-1200 °C," *Intermetallics*, Vol. 138, 107338 (2021).
33. W.G. Fahrenholtz, G.E. Hilmas, I.G. Talmy, and J.A. Zaykoski, "Refractory diborides of zirconium and hafnium," *J. Am. Ceram. Soc.*, vol. 90, pp. 1347–64 (2007).
34. A. Kumar, D. Rajdev, and D.L. Douglass, "Effect of Oxide Defect Structure on the Electrical Properties of ZrO₂," *J. Am. Ceram. Soc.*, vol. 55, pp. 439–45 (1972).
35. Manab Mallik, Sabyasachi Roy, K.K. Ray and R. Mitra, "Effect of SiC content, additives and process parameters on densification and structure-property relations of pressureless sintered ZrB₂-SiC composites," *Ceram. Inter.*, vol. 39(3), pp. 2915-32 (2013).
36. I. Barin, *Thermochemical Data of Pure Substances*, vol. 55, 1997.
37. Manab Mallik, Ansu J. Kailath, K.K. Ray, and R. Mitra, "Effect of SiC content on electrical, thermal, and ablative properties of pressureless sintered ZrB₂-based ultrahigh temperature ceramic composites," *J. Eur. Ceram. Soc.*, vol. 37 (2), pp. 559-72 (2017).
38. M. Suzuki, S. Sodeoka, T. Inoue, Structure control of plasma sprayed zircon coating by substrate preheating and post heat treatment, *Mater Trans. JIM*, vol. 46, 669–674 (2005).
39. R. Mitra, S. Upender, M. Mallik, S. Chakraborty, K.K. Ray, "Mechanical, thermal, and oxidation behaviour of zirconium diboride based ultra-high temperature ceramic composites," *Key Eng. Mater.*, vol. 395, pp. 55-68 (2009).
40. Manab Mallik, K.K. Ray, and R. Mitra, "Effect of Si₃N₄ addition on compressive creep behavior of hot pressed ZrB₂-SiC composites," *J. Am. Ceram. Soc.*, vol. 97(9), pp. 2957-64 (2014).

41. Sunil Kumar Kashyap and Rahul Mitra, “Densification behavior involving creep during spark plasma sintering of ZrB₂-SiC based ultra-high temperature ceramic composites,” *Ceram. Inter.*, vol. 46, pp.5028-5036 (2020).
42. Sunil Kumar Kashyap, Kasturi Sala and Rahul Mitra, “Oxidation resistance and evolution of multi-layered oxide scale during isothermal and cyclic exposure of ZrB₂-SiC-LaB₆ composites at 1300°C-1500°C,” *Metall. Mater. Trans. A* (2022) (In Press) <https://doi.org/10.1007/s11661-021-06501-4>.
43. Sunil Kumar Kashyap, Ankit Kumar and Rahul Mitra, “Kinetics and evolution of oxide scale during various stages of isothermal oxidation at 1300°C in spark plasma sintered ZrB₂ - SiC - LaB₆ composites,” *J. Eur. Ceram. Soc.*, vol. 40, pp. 4997-5011 (2020)
44. Sunil Kumar Kashyap and Rahul Mitra, “Microstructure and composition of multi-layered oxide scale evolved during isothermal exposure of ZrB₂-SiC-LaB₆ composite to air at 1500°C”, *Phil. Mag. Lett.*, vol. 201(7), pp. 265-276 (2021).